MICROWAVE DEVICE CHARACTERIZATION

BY

MYAT MYITZU SOE (B.E (Electronics), Y.T.U)

DEPARTMENT OF ELECTRICAL ENGINEERING

A THESIS SUBMITTED FOR THE DEGREE OF

MASTER OF ENGINEERING

NATIONAL UNIVERSITY OF SINGAPORE

2003

ACKNOWLEDGEMENTS

I would like to express my sincere gratitude to my supervisors, Prof. Leong Mook Seng and Dr. Ooi Ban Leong of the National University of Singapore (NUS) for their invaluable guidance and suggestions and patience throughout my pursuing of postgraduate program.

I also like to express the special thanks to lab technologists, Ms. Lee Siew Choo, Mr. Sing Chen Hiong both from the Microwave Lab, and Mr. Ng Chin Hock from RSPL Lab for their support and assistance rendered in the lab.

Special thanks go to Mr. Ho Min Jing Kevin and Mr. Yeo Museng for their support and valuable discussions during my early days at RSPL.

Last but not least, I would also like to thank my parents and my husband who are always encouraging, sacrificing, supportive and understanding.

SUMMARY

The emerging applications of wireless communications call for an effective low-cost approach to the microwave and RF packaging so as to meet the demand of the commercial market place. To ensure a good package design, development of the characterization techniques for surface mounted packages is thus necessary so as to predict their parasitic behavior at Microwave and RF frequencies. There is very little report on characterizing the multi-conductor leads, most especially, the coupling effect between near and neighboring pins of the microwave and RF packages.

This thesis investigates a unique systematic approach for on-wafer characterization and measurement of the inter-couplings of Leads of the low cost plastic packages, using the HP 8510 C, Vector Network Analyzer in conjunction with the air-coplanar wafer probes. For the first time, a whole series of novel coplanar package adapters for multi-conductors characterization has been developed. A set of electrical standards, based on TRL calibration scheme, has been designed for the calibration of the VNA by using Zealand Software, IE3D. Following the calibration standards, a special pattern is designed on the Taconic substrate to mount the package under test. This unique pattern consists of two parts, namely interconnects which make proper transition between the different pitches of the probe tips and the package pins under test and the patch on which the other part of the package is mounted. The first step of calibration only eliminates the imperfections where the probes touch interconnects. In order to obtain only the scattering parameters of the package, the scattering parameters of the pattern including interconnects are de-embedded out. The response of interconnect structures are measured and collected. Then, the package is attached to the patterned substrate using epoxy soldering cream. The Leads under test

as well as neighboring Leads are wire bonded to the die pad of the package, which provides common grounding. Verification of the consistency of the standards is made by measuring a line standard and there is good agreement between measured and simulation results. Then, the test piece is measured and characterized, and the response of the package is de-embedded.

Lump element as well as transmission line modeling of the package has been conducted using the MDS optimizer, until the response of the measured data is good in agreement with the response of predicted equivalent circuit. Utilizing the TSSOP, thin small shrink outline package, as the test piece, a new approach of multiconductor transmission line measurement and characterization technique has been developed.

TABLE OF CONTENTS

Table of Contents

LIST OF FIGURES

LIST OF TABLES

LIST OF SYMBOLS AND ABBREVIATIONS

ϕ	- Electric Potential
Φ	- Flux
λ	- Wavelength
λ_g	- Guide Wavelength
γ	- Propagation Constant
α	- Attenuation Constant
β	- Phase Constant
μ	- Permeability
μ_o	- Free-space Permeability
μ_r	- Relative Permeability
ε	- Permittivity
ε_o	- Free-space Permittivity
ε_r	- Relative Permittivity
$\overline{A}$	- Vector Magnetic Potential
$\overline{B}$	- Magnetic Flux Density
$\overline{E}$	- Electric Field
$\overline{H}$	- Magnetic Field

ACPW	- Asymmetrical Coplanar Waveguide
CAD	- Computer Aided Design
CPA	- Coplanar to Waveguide Adapter
CPS	- Coplanar Strip
CPW	- Coplanar Waveguide
DUT	- Device Under Test
IE3D	- Zealand IE3D (2.5D) Simulator
MDS	- Microwave and RF Design System
MILS	- Mili Inches
MMIC	- Monolithic Microwave Integrated Circuit
TEM	- Transverse Electromagnetic Mode
TRL	- Thru-Reflect-Line
TSOP	- Thin-Small-Outline Package
TSSOP	- Thin-Shrink-Small-Outline Package
VNA	- Vector Network Analyzer (HP 8510 C)
[T]	- Measured S-parameter matrix for Thru connection
[R]	- Measured S-parameter matrix for Reflect connection
[L]	- Measured S-parameter matrix for Line connection

Chapter One

Introduction

This thesis gives some general information about the usefulness of the characterization techniques using TRL Calibration procedures to characterize the surface-mountable plastic packages. This method is demonstrated by characterizing the TSSOP 16 pins lead counts plastic package. After a brief review, the detail process of the characterizing and modeling techniques performing on the TSSOP package, will be presented and discussed.

1.1 General Review

1.1.1 Introduction to Package Characterization

The application of wireless communications requires effective low-cost approaches to Microwave and RF packaging. One of the cost-effective solutions, to produce smaller, more efficient, less expensive electronic components for high frequency applications, is to use the surface-mountable plastic packages. Those packages contain inevitable parasitic elements at high frequency.

In microwave applications, the electromagnetic effects cannot be neglected and the performance limiting factors such as the resistive loss, losses in interconnects as

well as the coupling between the transmission lines must be taken into account. As a result, the calibration techniques using coplanar-waveguide-to-package adapter in conjunction with TRL calibration method is used to de-embed the response of the adapters from the measured s-parameters. So that the equivalent circuit which can be incorporated in a circuit simulator, can be extracted.

Surface-mounted plastic packages come in various types, sizes and grounding schemes. In this project, the electrical properties of thin shrink small outline package, TSSOP 16 pins package used as housing for MMIC circuits will be investigated. First of all, the process of the designing the special interconnects and electrical standards based on the physical constraints of the package dimensions as well as the dimension of the air-coplanar probes are discussed.

1.1.2 Structure and Features of TSOP 16 pins count Package

The TSSOP packages offer smaller body sizes and smaller lead pitches with package thickness of 0.9 mm over standard packages [see Figure 1.1(a)]. Body sizes are 3.0mm, 4.4 mm and 6.1 mm in general. Lead counts vary from 8 to 56. Standard lead pitch is 0.65 mm. In this project, the TSSOP 16 pins count package of the body size of 4.4 mm and pitch of 0.65 mm is used in the experiments [see Figure 1.1(b),(c),(d)]. The comparison of the dimensions of the package from the physical measurements and from the data sheet is shown in the Table 1.1.

The packages were made from plastic housings with lead-frame technology and gull-wing pins. The heat slug extends from the die pad inside the package to the mounting substrate to provide a ground plane as well as a thermal path to the substrate.

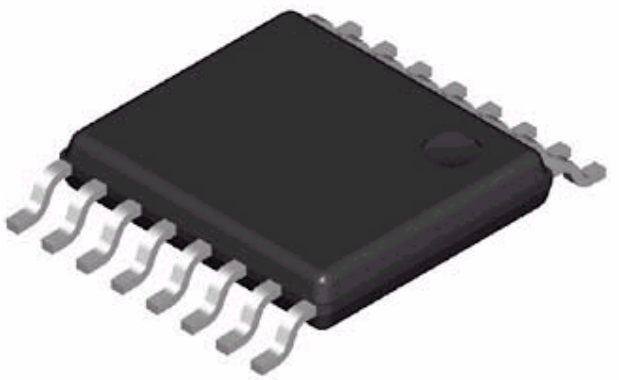

Figure 1.1 (a) Typical TSSOP 16 pins Package Geometry : physical model

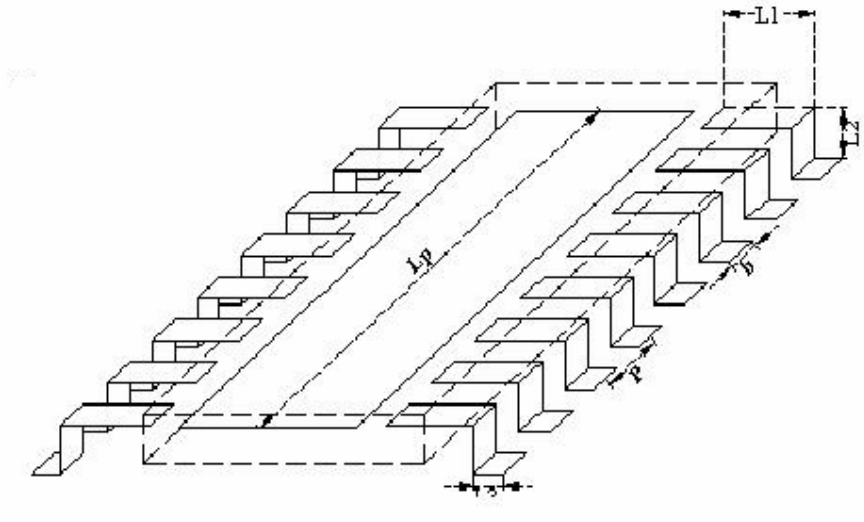

Figure 1.1 (b) Typical TSSOP 16 pins Package Geometry: Perspective View

Continued on next page.

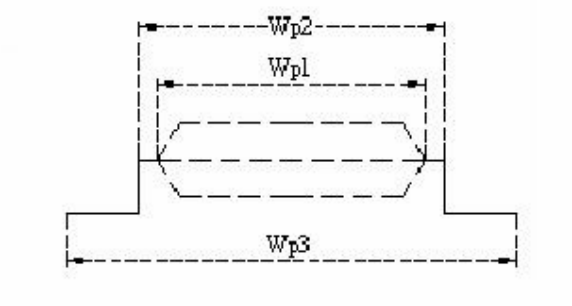

Figure 1.1 (c) Typical TSSOP 16 pins Package Geometry : Side View

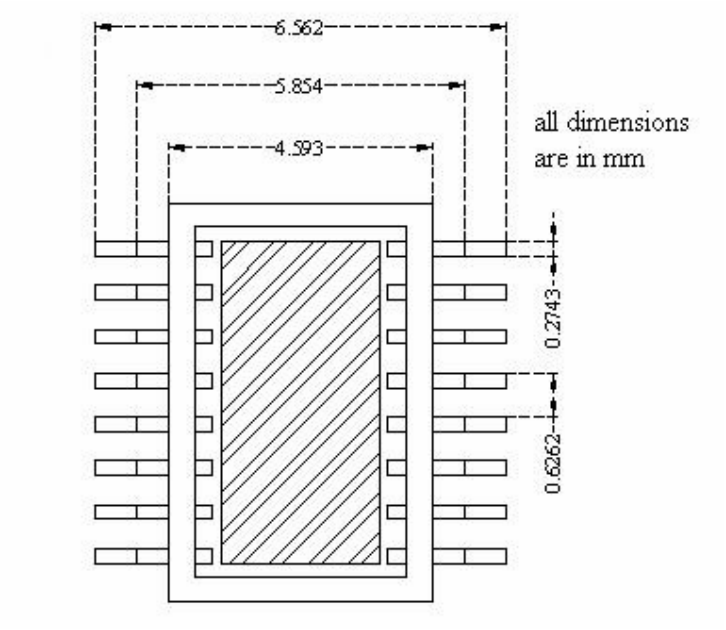

Figure 1.1 (d) Typical TSSOP 16 pins Package Geometry : Top View and Dimensions

Dimensions are in mm	Physical Measurements	From Data Sheet
Body Length (Lp)	4.82	5
Package Height	1.1	0.9
Body Size (Wp1)	4.593	4.4
Package Size (Wp3)	6.562	6.4
Width of the Pin	0.2743	0.3
Pitch of the Pin	0.6262	0.65
L1 (see Fig 1.1 a)	0.53	0.5
Height of the Pin (L2)	0.25	0.3
L3 (see Fig 1.1 a)	0.621	0.6

Table(1.1) Comparison of the dimensions of the package from the physical measurements and from the data sheet

1.1.3 Structure and Dimensions of Air Coplanar Wafer Probes

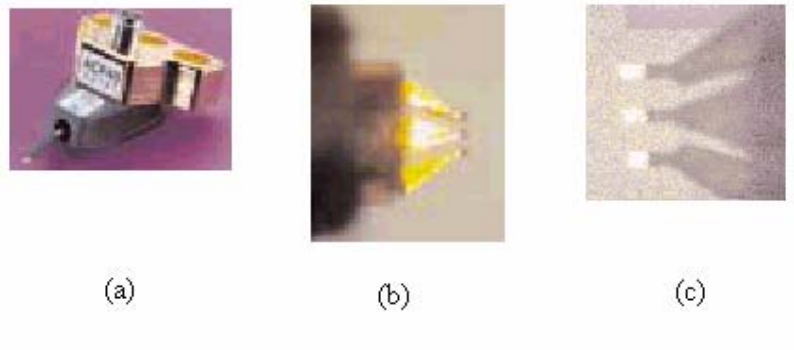

Figure (1.2) Air-coplanar Wafer Probe (a) Wafer Probe Structure (b) Probe Viewing (c) Properly Planarized Probe

A broad range of tip configurations are available. They include the high performance Ground-Signal-Ground (G-S-G) configuration, the Ground-Signal (G-S) and Signal-Ground (S-G) configurations, and the dual tip configuration of G-S-G-S-G. There are varieties of center-to-center contact spacing or the probe pitch and the standard of the pitch varies from $100\,\mu$ to $250\,\mu$. In this project, the GSG probe of $250\,\mu$ configuration is used, so as to compromise the differences in dimensions of the pitch of the package leads and the probe. The typical GSG air-coplanar probe and its details are shown in Figures (1.3) (a), (b) and (c).

1.1.4 Objectives and Methodologies

Increased end-application densities and shrinking product sizes demand more from IC packages. Plastic Packages give designers the needed margin for designing and producing high performance products such as telecom, disk drives, pagers, wireless, CATV/RF modules, radio, aerospace, automotive, industrial and other applications including Bluetooth.

Although these packages are designed to meet the critical requirements in microwave and RF applications, they have inevitable parasitic at high frequency. The main objective of this project is to introduce a unique method to predict these parasitic behaviors of these packages at microwave frequency to improve the package design. This method is developed based on the TRL (Thru-Reflect-Line) calibration method.

The steps used are as follows:

(a) Design the proper interconnects for TRL Calibration

(b) Measure the Package

(c) Extract the parasitic from measured data

(d) Extract the electrical model of the package using CAD Tools and Numerical Equations,

Figure (1.3) shows a flowchart for the methodology used in this project. Because of the size constraints, proper procedure for mounting the interconnects in order to make proper transitions between the wafer-probes and the package leads are designed.

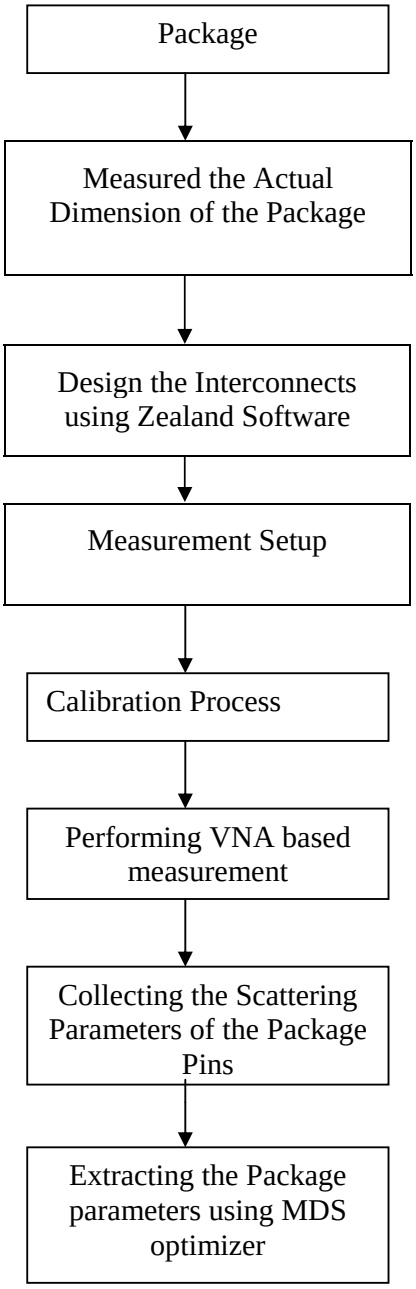

Figure (1.3) Methodology used in this project.

1.2 Contents of This Thesis

This Thesis, which is organized in five chapters, gives a new idea and unique way to characterize and predict the parasitic behavior of plastic packages using TRL calibration method.

The first chapter gives the general information of package characterization, the adapted general structure of the TSSOP package, as well as the structure and properties of the air-coplanar probes (wafer probes) used as one of the measurement tools.

The theoretical background of the two most common transmission line which are used in design considerations for the calibration standards and the implementation of TRL single line as well as TRL for multi-conductor transmission lines are presented in Chapter 2. Chapter 3 explains the measurement procedures and characterization of the package Leads in details using the Vector Network Analyzer and air-coplanar probes. This chapter emphasizes on the single lead measurement as well as multi-lead measurements and extractions of the S-parameters. Chapter 4 gives the lump element modeling from the collected S-parameters of the leads. This Chapter gives an in-depth of the single lead modeling as well as the multi-lead modeling technique.

Finally, a conclusion is drawn at Chapter 5.

1.3 Some Original Contributions

The objective of this thesis is to introduce a whole new method to characterize and model the low-cost surface-mount plastic packages. In this project, TSSOP packages are used as test components to experiment the method. For the first step, the interconnects enabling the proper transitions between the package Leads and wafer-probes are designed and fabricated using photolithography technique. On-wafer measurements of the packages using the HP 8510 C, Vector Network Analyzer in conjunction with air-coplanar probes are performed and the electrical model of the package is extracted.

The development of novel characterization technique for surface mounted packages has been introduced so as to predict the parasitic behavior of packages and RF frequencies. As for the first step of this thesis, a single lead characterization of TSSOP 16 leads package has been carried out. The characterization of multi-conductor leads, most especially, the coupling effects between near and neighboring pins of the microwave and RF packages is next carried out.

In this research, a systematic approach of on-wafer characterization of a TSSOP package has been developed. For the first time a whole series of novel coplanar package adapter for single lead characterization and multi-conductors characterization has been designed. Utilizing the designed interconnects, transmission line modeling as well as lump element modeling of the TSSOP packages have been performed.

Contributions:

As a result of this research, the following paper has been published.

(a) M. S. Leong, B. L. Ooi and M. M. Soe, "A systematic on-wafer characterization technique for surface- mounted microwave and RF packages", presented at The PACIFIC RIM/ International, Intersociety, Electronic Packaging, Technical /Business Conference & Exhibition, July 8-13,2001.Hyatt Regency Kauai. Kauai, Hawaii, USA

Chapter Two

Design Considerations and Implementation of the Method

In this chapter, the theoretical background of the two most common transmission line structures for design considerations for the calibration standards and the implementation of TRL single line as well as TRL for multi-conductor transmission lines are presented.

2.1 Theoretical Background

The Microwave frequency refers to frequency range from 300 MHz to 300 GHz range which in turns in electrical wavelength from 1 m to 1 mm. Microwave circuits are distributed circuits in which the dimensions of the circuit component is at least some fraction of the wavelength of the operating frequency. So that the circuits must be capable of describing the action of lumped elements as well as distributed parameters.

2.1.1 Transmission Line Theory

In many ways, transmission line theory plays a big role to fill up the requirements between field analysis and basic circuit theory. So that, it is very important in microwave network analysis. As shown in Figure (2.1), a transmission line is often represented in two wire lines as for schematically for transmission lines always have at least two conductors. Transmission line in Figure 2.1(a) can be modeled as lumped element circuit as shown in Figure2.1 (b). And the R, L, C and G are per unit length and represent as series resistance per unit length in ohms, series inductance per unit length in hennery, shunt capacitance per unit length in Farrad and shunt conductance per unit length in mho, respectively.

Generally, L defines as the self-inductance of the transmission lines and C represents the close proximity of the two conductors. Both R and G represent losses, the resistance due to finite conductivity of the conductors and the dielectric loss in the material between two conductors, respectively. A finite length transmission line can be modeled as a cascade of sections of the form of Figure 2.1(b).

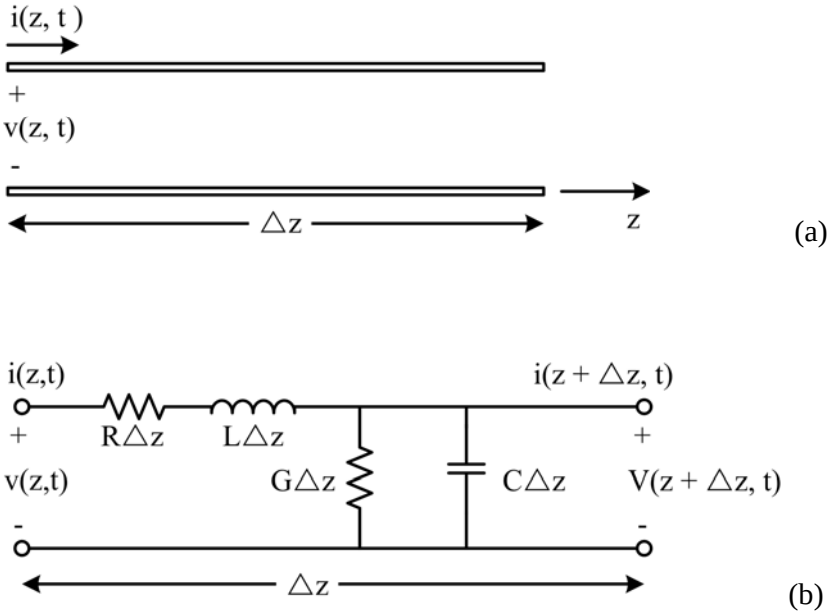

Figure (2.1) Representation and Equivalent Circuit of a basic transmission line

Applying Kirchhoff's Voltage Law to the Figure (2.1b):

$$v(z,t) - R\Delta z i(z,t) - L\Delta z \frac{\partial i(z,t)}{\partial t} - v(z+\Delta z,t) = 0\,, \qquad (2.1)$$

Applying Kirchoff's current Law :

$$i(z,t) - G\Delta z v(z+\Delta z,t) - C\Delta z \frac{\partial v(z+\Delta z,t)}{\partial t} - i(z+\Delta z,t) = 0\,, \qquad (2.2)$$

Dividing (2.1) and (2.2) by Δz, and taking $\Delta z \to 0$,

$$\frac{\partial v(z,t)}{\partial z} = -Ri(zmt) - L\frac{\partial i(z,t)}{\partial t}, \tag{2.3}$$

$$\frac{\partial i(z,t)}{\partial z} = -Gv(z,t) - C\frac{\partial v(z,t)}{\partial t}, \tag{2.4}$$

So that the time-domain form of the transmission lines can be obtained. For the sinusoidal steady-state condition, with cosine based phasors, (2.3) and (2.4) can be simplified to (2.5) and (2.6) respectively.

$$\frac{dV(z)}{dz} = -(R + jwL)I(z), \tag{2.5}$$

$$\frac{dI(z)}{dz} = -(G + jwC)V(z), \tag{2.6}$$

These two equations could be solved to get the equations for V(z) and I(z).:

$$\frac{d^2 v(z)}{dz^2} - \gamma^2 V(z) = 0, \tag{2.7}$$

$$\frac{d^2 I(z)}{dz^2} - \gamma^2 I(z) = 0, \tag{2.8}$$

where $\gamma = \alpha + j\beta = \sqrt{(R + j\omega L)(G + j\omega C)}$, (2.9)

which is the complex propagation constant in function of frequency.

Thus, solutions to equations (2.7) and (2.8) can be obtained as:

$$V(z) = V_o^+ e^{-\gamma z} + V_o^- e^{\gamma z}, \tag{2.10}$$

$$I(z) = I_o^+ e^{-\gamma z} + I_o^- e^{\gamma z}, \tag{2.11}$$

where the $e^{-\gamma z}$ refers to the wave propagation in +z direction, and $e^{\gamma z}$ refers to the wave propagation in –z direction. Applying (2.5) to (2.10),

$$I(z) = \frac{r}{R + j\omega L}[V_o^+ e^{-\gamma z} - V_o^- e^{\gamma z}], \tag{2.12}$$

Comparing (2.12) and (2.11) gives

$$z_o = \frac{R + j\omega L}{\gamma} = \sqrt{\frac{R + j\omega L}{G + j\omega C}}, \tag{2.13}$$

Thus, the voltage and current of the line can be related as

$$\frac{V_o^+}{I_o^+} = Z_o = \frac{-V_o^-}{I_o^-},$$

which can be rewritten as

$$I(z) = \frac{V_o^+}{Z_o} e^{-\gamma z} - \frac{V_o^-}{Z_o} e^{\gamma z}, \tag{2.14}$$

In time-domain, the wave forms can be represented as:

$$v(z,t) = \left|V_o^+\right| Cos(\omega t - \beta z + \phi^+) e^{-\alpha z} + \left|V_o^-\right| Cos(\omega t - \beta z + \phi^-) e^{\alpha z}, \tag{2.15}$$

where $\phi^{\pm}$ is the phase angle of the complex voltage $V_o^{\pm}$.

The transmission line parameters can also be derived in terms of the electric and magnetic fields of the transmission line. Let us assume that one unit length of a uniform transmission line as shown in Figure (2.2) with fields $\overline{E}$ and $\overline{H}$ is under consideration, where **S** is the cross-sectional surface area of the line.

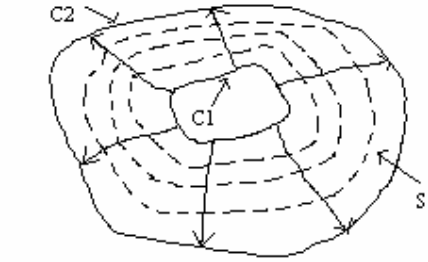

Figure (2.2) Fields Lines on arbitrary TEM Line

Let the voltage and current of the line be $V_o e^{\pm j\beta z}$ and $I_o e^{\pm j\beta z}$. The magnetic stored energy for this line is

$$W_m = \frac{\mu}{4}\int_s \overline{H}\cdot\overline{H}^* ds = L\frac{I_o^2}{4},$$

Thus, self-inductance per unit length is

$$L = \frac{\mu}{|I_o|^2}\int_s \overline{H}\cdot\overline{H}^* ds \quad \text{H/m} \tag{2.16}$$

The time average stored electric energy for this line is

$$W_e = \frac{\varepsilon}{4}\int_s \overline{E}\cdot\overline{E}^* ds = C|V_o|^2,$$

Thus, the capacitive per unit length is

$$C = \frac{\varepsilon}{|V_o|^2}\int_s \overline{E}\cdot\overline{E}^* ds, \tag{2.17}$$

The power loss per unit length due to finite conductivity of the metallic conductors is

$$P_c = \frac{R_s}{2}\int_{C1+C2} \overline{H}\cdot\overline{H}^* dl = R\frac{|I_o|^2}{2}, \tag{2.18}$$

Assuming $\overline{H}$ is tangential to S, the series resistance per unit length of line is

$$R = \frac{R_s}{|I_o|^2} \int_{C1+C2} \overline{H} \cdot \overline{H}^* dl \quad \Omega / m \tag{2.19}$$

where $R_s = \frac{1}{\sigma \delta_s}$, surface resistance of the conductors and C1+C2 represent the integration paths over the conductor boundaries.

The time average power in the lossy dielectric is

$P_d = \frac{\omega \varepsilon''}{2} \int_s \overline{E} \cdot \overline{E}^* ds = G \frac{|V_o|^2}{2}$ where ε'' is the imaginary part of the complex dielectric constant $\varepsilon = (\varepsilon' - j\varepsilon'') = \varepsilon'(1 - j \tan \delta)$

Thus the shunt conductance per unit length is

$$G = \frac{\omega \varepsilon''}{|V_o|^2} \int_s \overline{E} \cdot \overline{E} ds \text{ S/m} \tag{2.19}$$

2.1.2 Coplanar Transmission Lines

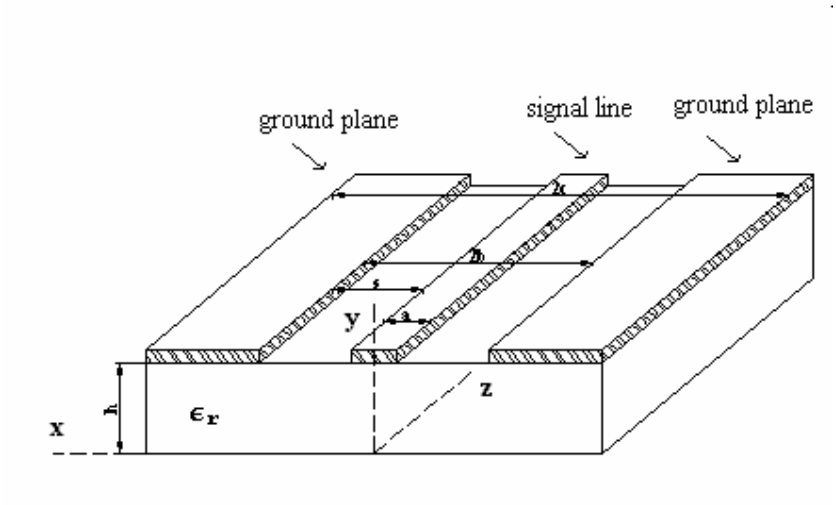

Figure (2.3) Coplanar Line on a finite thickness dielectric substrate

The coplanar lines are transmission lines those all the conductors lie on the top surface of the dielectric substrate. Coplanar lines are used in such a way to mount lumped active or passive components which are in coplanar nature. Moreover, coplanar lines are commonly used in MMIC circuits. The performance of coplanar line is comparable to microstrip lines with guided wavelength, dispersion and losses. Coplanar line has some disadvantages such as parasitic modes, lower power-handling capability, and field non-confinement.

A typical coplanar wave guide with finite ground plane is shown in Figure(2.4). It consists of a signal conductor of width **a** placed on the top of the substrate. Ground planes are situated on each side of the signal conductor separated from that signal line by the distance **s**.

Since the air-coplanar probes to measure the package lead are in **G-S-G** coplanar structure, we choose the coplanar structure as the basic configuration in designing the calibration standards as well as the pattern on the substrate to mount the package on. In this work, this basic structure of coplanar waveguide is mainly used in designing standards for single line TRL calibration method.

2.1.3 Coplanar Strips

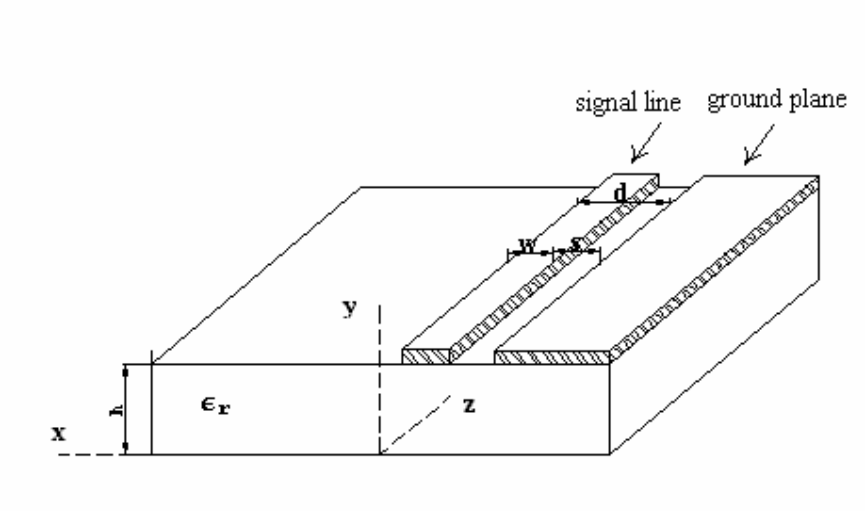

Figure (2.4) Coplanar Strips

The configuration of double-strip coplanar waveguide with infinitely wide ground conductors is shown in the figure (2.4). It is composed of a signal line with width **w** and it is separated by the distance **s** from the ground plane. As seen in the figure, all the conductors are placed on the top side of the substrate.

2.1.4 Coplanar Strips with lateral ground planes

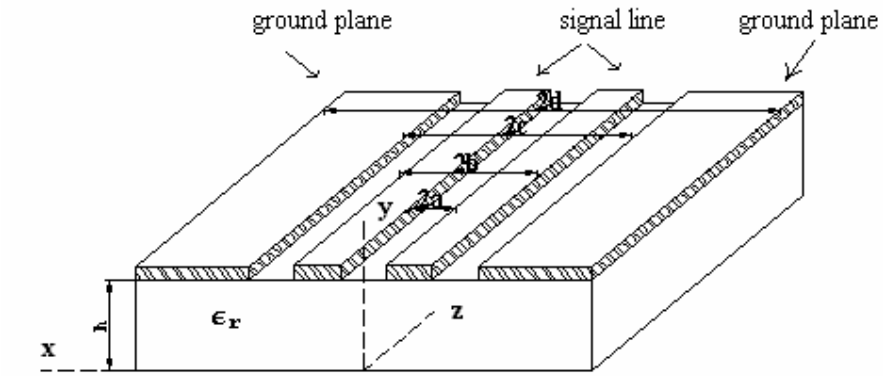

Figure (2.5) Coplanar Strips with lateral ground planes

The configuration of CPS with lateral ground planes is shown in figure (2.5). This structure reduces line to line coupling. In this thesis, this structure is used in designing of the interconnects for the measurement of coupling of the adjacent pins of the package.

2.1.5 Microstrip Transmission Lines

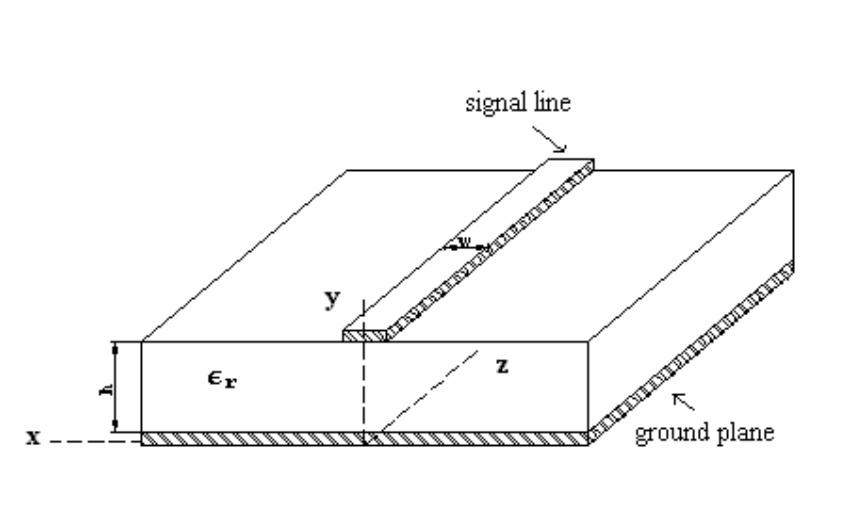

Figure (2.6) Microstrip Line on a finite thickness dielectric substrate

Microstrip line is a common planar transmission line. The signal conductor lies on the top surface of the dielectric substrate and is backed by a conductor, ground plane on the bottom surface of the substrate. Microstrip lines are used in MICs for lumped active or passive components can be mounted in the circuits. Moreover, microstrip lines are commonly used in MMIC circuits. Due to dielectric-air interface, the mode of propagation in a microstrip is a non-TEM hybrid mode. A typical microstrip line is shown in Figure(2.6). It consists of a signal conductor of width **w** placed on the top of the substrate. Ground plane is situated on the back of the dielectric substrate.

In this thesis, the package leads are represented with lump elements as well as microstrip transmission lines for transmission line representation can capture parasitic of the package at high frequency more accurately.

2.2 Implementation of TRL

For on-wafer scattering parameter measurement, the results are referenced to the fundamental on-wafer impedance standards used in VNA calibration. Standards are designed according to the characteristics of the VNA and the wafer probes, so that the operations of the probes and VNA can be properly assessed.

2.2.1 TRL Calibrations

The calibration of the network analyzer using the Thru-Reflect-Line (TRL) technique is considered by the application of the signal flow graphs. The general configuration to measure the S-parameters of a two-port device at the indicated reference planes is shown in the Figure (2.7) .In the Figure (2.7), the effects of losses, and phase delays caused by the connectors, cables, and transitions which are used to connect the DUT to the analyzer are lumped in a two-port error box placed at each port between the actual reference plane and the desired reference plane for the two-port DUT. The calibration procedure is used to characterize the error boxes before measurement of the DUT. Thus the error-corrected S-parameters of the DUT can be obtained from the measured data.

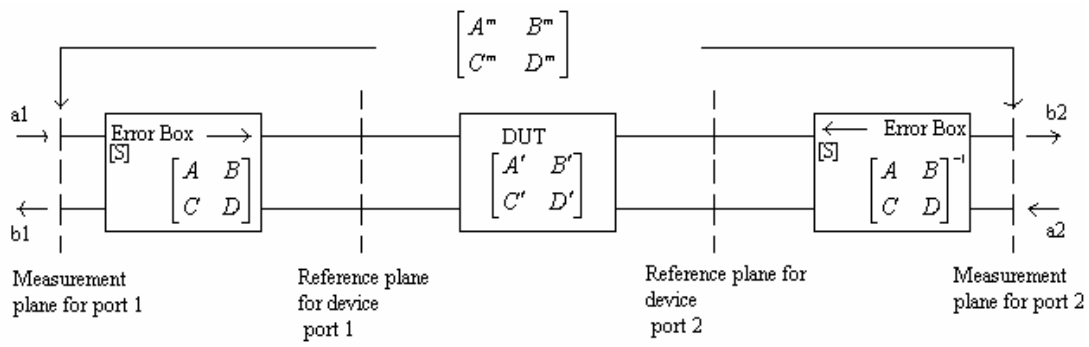

Figure(2.7) Block diagram of the two-port device network analyzer measurement

Calibrating the VNA with the application of the TRL scheme uses three basic connections to allow the error boxes to be characterized completely. These connections are Thru, Reflect and Line connections. Their connection block diagrams and the signal flow graphs are shown in Figure (2.8)-Figure (2.10).

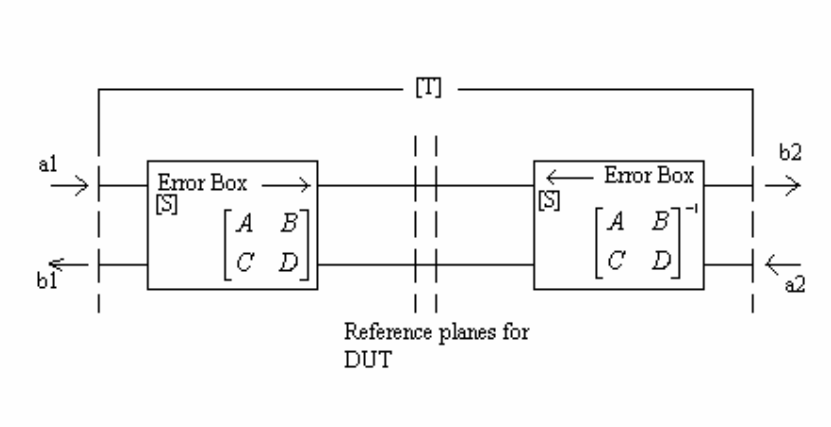

Figure(2.8.a) Block Diagram for the Thru Connections

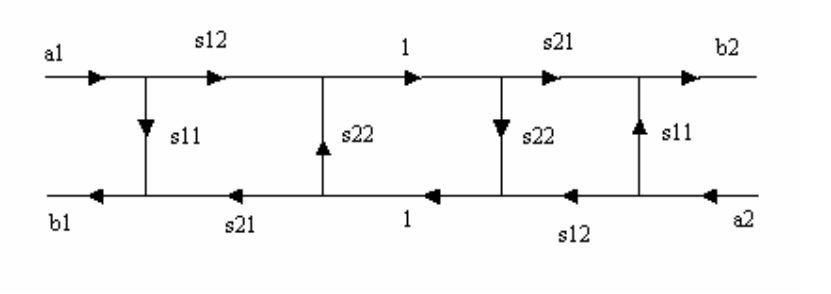

Figure(2.8.b) Signal flow graph for the Thru Connections

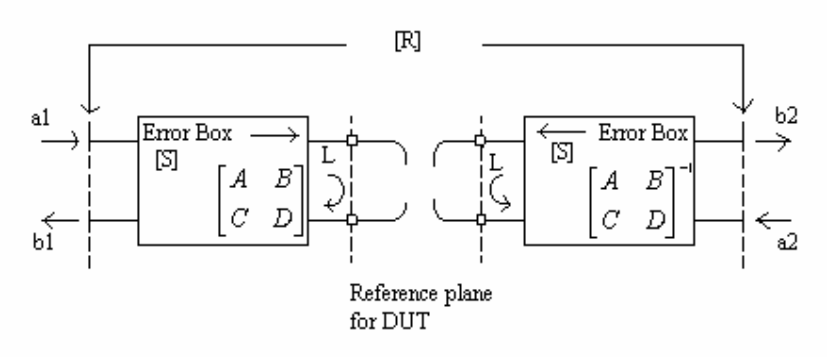

Figure(2.9.a)Block Diagram for Reflect connection

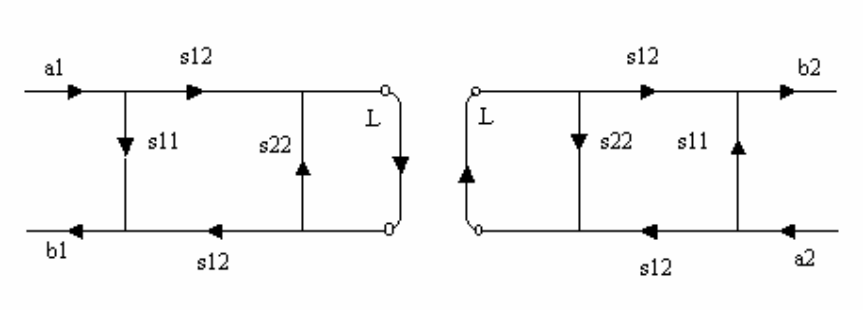

Figure(2.9.b) Signal flow graph for the Reflect Connections

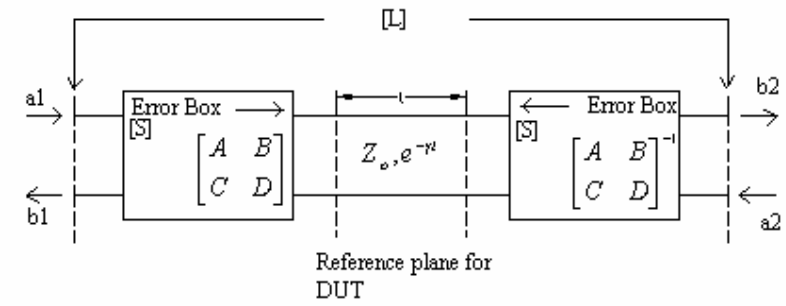

Figure(2.10.a) Block diagram for the Line connection

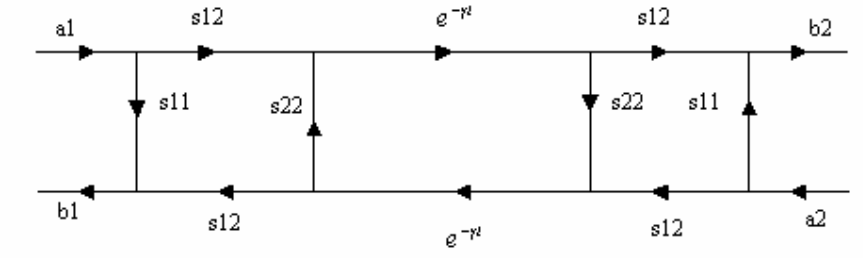

Figure (2.10.b) Signal flow graph for the Line Connection

The Thru connection is made by directly connecting port 1 and port 2 at the desired reference planes. The Reflect connection is made by terminating with a large reflection coefficient, Γ_l, such as nominal open or short. The exact value of Γ_ℓ for it would be determined by the calibration procedure. The line connection is made by connecting the port 1 and port 2 together by a length of matched transmission line. It is not necessary to know the length of the line and it is not required that the line is lossless. These parameters would be determined by the calibration.

The equation to find the S-parameters for the error-boxes in the TRL calibration procedure could be derived by using signal flow graphs. For simplicity, set the same characteristic impedance for port 1 and port 2, and the error boxes are reciprocal and identical for both ports. The error boxes are characterized by S-matrix [S] as well as ABCD matrix.

Considering error boxes, $S_{12} = S_{21}$ for both of the boxes. Since they are also symmetrically connected, there are inverse relation between the ABCD matrices of the error boxes for port 1 and port 2. The measured S-parameters for the Thru, Reflect, and Line connections are denoted as [T], [R], and [L] respectively.

From the Thru connections as shown in the Figure (2.8.a) and Figure (2.8.b), the signal flow graph could be reduced to obtain the measured S-parameters at the measurement planes, in terms of the S-parameters of the error boxes, as follows:

$$T_{11} = \frac{b_1}{a_1}\bigg|_{a_2 = 0} = S_{11} + \frac{S_{11} \quad S^2{}_{12}}{1 \quad - \quad S^2{}_{22}}, \tag{2.21}$$

$$T_{12} = \frac{b_1}{a_2}\bigg|_{a_1 = 0} = \frac{S^2{}_{12}}{1 \quad - \quad S^2{}_{22}}. \tag{2.22}$$

By symmetry, $T_{22} = T_{11}$, and by reciprocity, $T_{21} = T_{12}$.

According to the Reflect connection shown in Figure (2.8.a) and its signal flow graph, the two measurement ports are effectively decoupled and $R_{12} = R_{21} = 0$. The following equation is easily deduced.

$$R_{11} = \frac{b_1}{a_1}\bigg|_{a_2 = 0} = S_{11} + \frac{S^2{}_{12} \quad \Gamma_l}{1 \quad - \quad S_{22}\Gamma_l} \tag{2.23}$$

By symmetry, $R_{22} = R_{11}$

From the Line connections as shown in the Figure (2.9.a) and Figure (2.9.b), the signal flow graph could be reduced to obtain the measured S-parameters at the measurement planes, in terms of the S-parameters of the error boxes, as follows:

$$L_{11} = \frac{b_1}{a_1}\bigg|_{a_2=0} = S_{11} + \frac{S_{22}\ S^2{}_{12}\ e^{-2\gamma l}}{1 - S^2{}_{22}\, e^{-2\gamma l}}, \tag{2.24}$$

$$L_{12} = \frac{b_1}{a_2}\bigg|_{a_1=0} = \frac{S^2{}_{12}\, e^{-\gamma l}}{1 - S^2{}_{22}\ e^{-2\gamma l}}. \tag{2.25}$$

By symmetry , $L_{ss} = L_{11}$, and $L_{21} = L_{12}$.

By solving the above equations, the solution equations for S_{22} and e^{-rl} could be reduced as follows:

$$L_{12}e^{-2\gamma l} - L_{12}S^2{}_{22} = T_{12}e^{-\gamma l} - T_{12}S^2{}_{22}e^{-\gamma l}, \tag{2.26}$$

$$e^{-2\gamma l}(T_{11} - S_{22}T_{12}) - T_{11}S^2{}_{22} = L_{11}(e^{-2\gamma l} - S^2{}_{22}) - S_{22}T_{12}\ , \tag{2.27}$$

$$e^{-\gamma l} = \frac{L^2{}_{12} + T^2{}_{12} - (T_{11} - L_{11})^2 \pm \sqrt{[L^2{}_{12} + T^2{}_{12} - (T_{11} - L_{11})^2]^2 - 4T^2{}_{12}T^2{}_{12}}}{2\,L_{12}\ T_{12}}$$

(2.28)

$T_{11}, L_{11}, S_{22}, S_{11}$ *and* S_{12} could be deduced from the equation above as well as Γ_l and they are given as follows:

$$T_{11} = S_{11} + S_{22}T_{22} \ , \tag{2.29}$$

$$L_{11} = S_{11} + S_{22}L_{12}e^{-\gamma l} \ , \tag{2.30}$$

$$S_{22} = \frac{T_{11} - L_{11}}{T_{12} - L_{12}e^{-\gamma l}} \ , \tag{2.31}$$

$$S_{11} = T_{11} - S_{22}T_{12} \ , \tag{2.32}$$

$$S^{2}_{12} = T_{12}(1 - S^{2}_{22}) , \tag{2.33}$$

Thus Γ_l could be solved as follows:

$$\Gamma_l = \frac{R_{11} - S_{11}}{S^{2}_{12} + S_{22}(R_{11} - S_{11})} . \tag{2.34}$$

From equation (2.27) and (2.30)-(2.33), the S-parameters for the error boxes as well as unknown reflection coefficient Γ_l and the propagation factor, $e^{-\gamma l}$ could be obtained and the calibration procedure of TRL scheme is completed.

2.2.2 De-embedding

The measured S-parameter of DUT at the measurement reference planes as shown in the Figure (2.6) is collected. After using the TRL technique, this gives the S-parameters at the reference planes of the DUT. Since the two port networks are cascaded, all the S-parameter matrices are converted to ABCD parameter and ABCD parameter of the DUT is determined. In the following representation, ABCD parameters represent the parameters of the error boxes, $A'B'C'D'$ represent the

parameters of the DUT and $A^m B^m C^m D^m$ represent the parameters of the measured parameters. The equation of the measured overall S-parameters is shown in equation (2.34). Thus, using all the parameters obtained from equation (2.28)-(2.33), and converted them to ABCD parameters, the ABCD matrix of the DUT is de-embedded from the overall measured parameters, equation (2.35).

$$\begin{bmatrix} A^m & B^m \\ C^m & D^m \end{bmatrix} = \begin{bmatrix} A & B \\ C & D \end{bmatrix} \begin{bmatrix} A' & B' \\ C' & D' \end{bmatrix} \begin{bmatrix} A & B \\ C & D \end{bmatrix}^{-1}. \quad (2.35)$$

Thus the ABCD parameter of the DUT could be obtained.

$$\begin{bmatrix} A' & B' \\ C' & D' \end{bmatrix} = \begin{bmatrix} A & B \\ C & D \end{bmatrix}^{-1} \begin{bmatrix} A^m & B^m \\ C^m & D^m \end{bmatrix} \begin{bmatrix} A & B \\ C & D \end{bmatrix}. \quad (2.36)$$

2.2.3 Design of Electrical Standards for measurement of the pins of the opposite sides of the package

The measurement method used in this project is based on conventional TRL calibration method. TRL calibration method is a simple method for the calibration of devices for which matched loads are not available. Basically, this method requires three electrical standards such as a through connection, a high reflectivity termination and a uniform line which has the optimum electrical length of 90 degrees or an odd-multiple of a quarter-wavelength. Electrical Lengths near 0 degree or multiple of 90 degrees must be avoided or the solutions of the closed-forms could not be truly evaluated. A phase difference between 18 degrees and 162 degrees has been approved, however 30 degrees and 150 degrees phase difference are recommended. A through standard could be designed with a spacer value between 0 and $\lambda/4$.

The calibration kit is designed based on the TRL calibration technique [11,12], which consists of three transmission lines and a pair of two short circuits as reflects using CAD tool, IE3D. The TRL calibration standard and the interconnects for the calibration of the VNA for the measurement and characterization of the opposite side of the individual package lead [See Figure (2.11) & (2.12)]. Following the calibration standard is the pattern designed on the Alumina substrate to mount and measure the package.

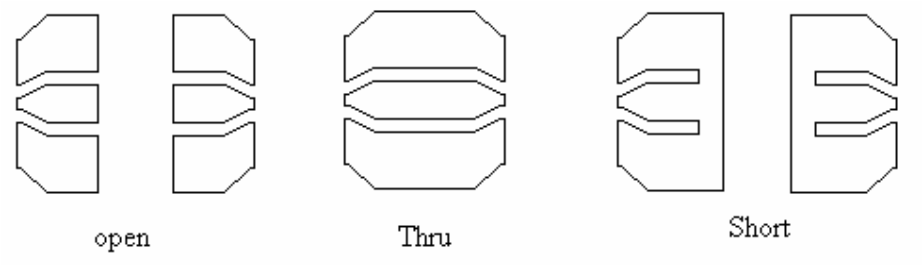

(a)

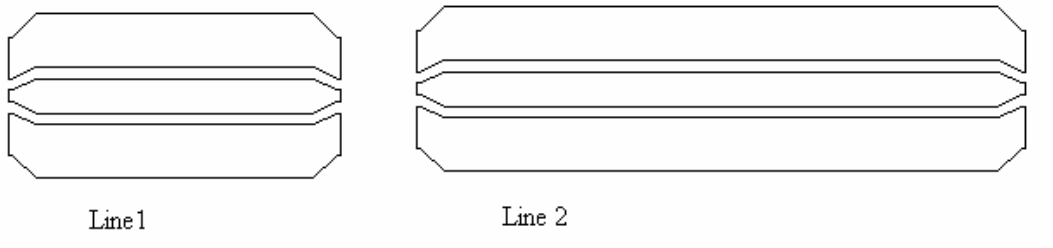

(b)

Figure (2.11) The layout of Coplanar waveguide to package adapter (CPA) calibration standards for enabling the measurement of the package pins without accounting for the inter-coupling between adjacent pins.

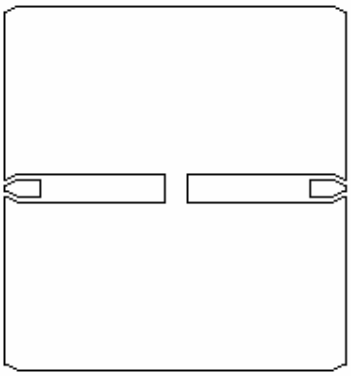

Figure (2.12) The patterned designed for package pin measurement without taking account into the inter-couplings between adjacent pins with CPA

The format of the CPA traces is ground-signal-ground, which is compatible with the configuration of the air coplanar probes. The CPAs are designed as taper structure so that the proper transition between the air coplanar probes used for IC measurements, which has the pitch dimension of 250 micron and the package pins which have the width of 10 mils, can be provided. The length of the tapered section is 12 mils in order to maintain the 50 ohm CPW structure. The slot width is uniform along the transition with 5 mils. The smaller width of the taper section is 5 mil in order to make proper transition with the probe width and the width of ground planes is 20 mils. The tapered section which is designed for compatibility with the probe dimension is extended 1.5 mils further, so that the probe will be able to sit and meet the 50 ohm CPW transmission lines. The larger dimension of the tapered section is 15 mils and the length is also extended to 34 mils enabling 12 mils package pin to sit properly.

Alumina substrate with the thickness of 25 mils and the dielectric constant of 9.96 is used to implement the standards. The conductivity of gold is $4.23 \times 10^7 \ \Omega / \mu m$.

THRU standard is specified to have an Offset Delay of 0 picosecond and operate over 1 GHz to 30 GHz, frequency range. A zero-length THRU can be used over any frequency span that the transmission medium can support. Since the Offset Delay of a zero-length thru is accurately known, it is typically used to set the reference plane. Reflect standard is a nominal zero-length short circuit. It is designed to have the Offset Delay of 0 picoseconds, and operate over 1 GHz to 30 GHz frequency range and only approximate phase information is required.

Since the transmission media exhibits linear phase, the following expression can be used to select a LINE with quarter wavelength line at the center frequency.

Start frequency = 1 GHz

Stop frequency = 30 GHz

Electrical Length (cm) = (LINE – THRU) (2.36)

= 15/[f1 (GHz) + f2(GHz)]

= 0.4838 cm

= l

To determine whether the LINE meets the conditions of acceptable insertion phase, the following expression can be used:

Phase (degree) = (360 * f* l) / c (2.37)

where c = 3×10^{10} cm/s

phase at 1 GHz = 6 degrees

30 GHz = 175 degrees

It is obvious that 0.4838 cm line does not meet the recommended insertion phase requirements between 20 and 160 degrees with respect to the THRU. In order to cover greater than 8:1 frequency span, multiple lines must be used. Since, the frequency span is less than 64:1, then two THRU/LINE pairs will be sufficient.

The desired frequency span must be divided, allowing a quarter wavelength LINE to be used over the lower portion of the frequency span and a second to be used for the upper band. The optimal break frequency is the geometric mean frequency of the start and stop frequency.

The break frequency = square root of (f1 * f2) (2.38)

= 5.477 GHz

Using equation (2.38) LINE standard 1 for low frequency regime (from 1 to 5.5 GHz) and LINE standard 2 for high frequency regime (from 5.4 to 30 GHz) are designed and the lengths are 2.32 cm and 0.4228 cm respectively. When defining the standards,the minimum frequency for high frequency regime is set to 5.4 GHz and the maximum frequency for low frequency regime, so that the overlapping at the boundary frequency of 5.477 GHz can be obtained.

The approximate Offset Delay can be computed as follows:

Offset Delay = Electrical Length (cm)/ c (cm/s) (2.39)

Calculated Offset Delays of the 2.32 cm line standard and 0.4228 cm line standard are 77.33 and 14.1 picoseconds respectively. Lines standards are fabricated and measured to verify whether the phase meets the recommended requirements. After class assignments and standards as shown in Table (2.1) and Table (2.2) and these values are entered into HP 8510 C registers. (Appendix A)

Standards		Offsets		Frequency (Hz)		Standard Label
No.	Types	Delay(Ps)	Zo (Ω)	min	max	
14	delay	0				Thru
15	delay	77.33	50	1	5.5	Line 1
16	delay	14.1	50	5.4	30	Line 2
18	short	0		1	30	Short

Table (2.1)CAL KIT Standard Definition for measurement of single lead

Standard Class Assignment	A	B	Standard Class Label
TRL THRU	14		THRU
TRL REFLECT	18		SHORT
TRL LINE	15	16	LINES

Table (2.2) Standard Class Assignments

The TRL calibration is performed on the CPA standards using the VNA, HP 8510 C. The IE3D digital simulation results of the s-parameter of the standards are shown in Figure (2.13).

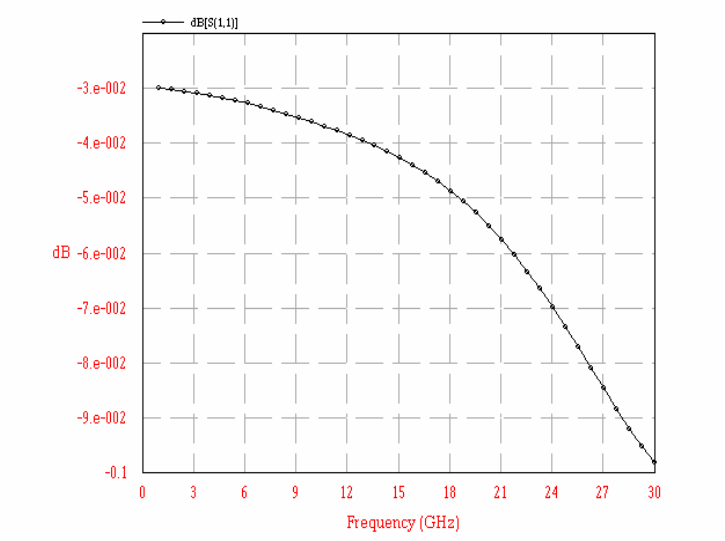

Figure 2.13(a) Magnitude of S11 of Short Standard

Since the Magnitude of S11 of Short Standard is approximately zero, the designed standards is perfectly can be used in the calibration process.

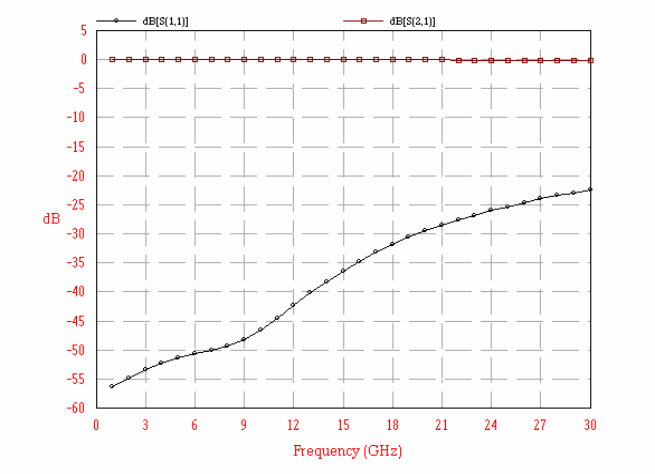

Figure 2.13 (b) Magnitude of S11 & S21 of Thru Standard

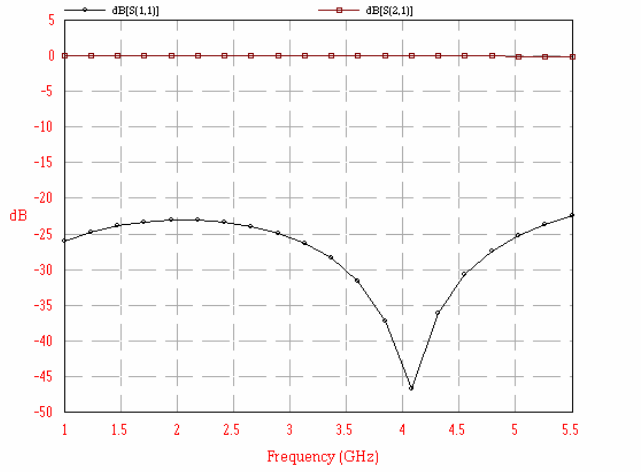

Figure 2.13 (c) Magnitude of S11 and S21 of Line standard

From the Fig 2.13 (b) and Fig 2.13 (c) the magnitudes of S21 of both Line and Thu standards are very much closed to zeros which means that there is no excitation of power in the process and the standards designed are stable and so as for magnitude of S11 of both the above mentioned standards, Line and Thru.

From above figures, it should be confirmed that the standards designed are stable to calibrate the analyzer and imperfections of the probes.

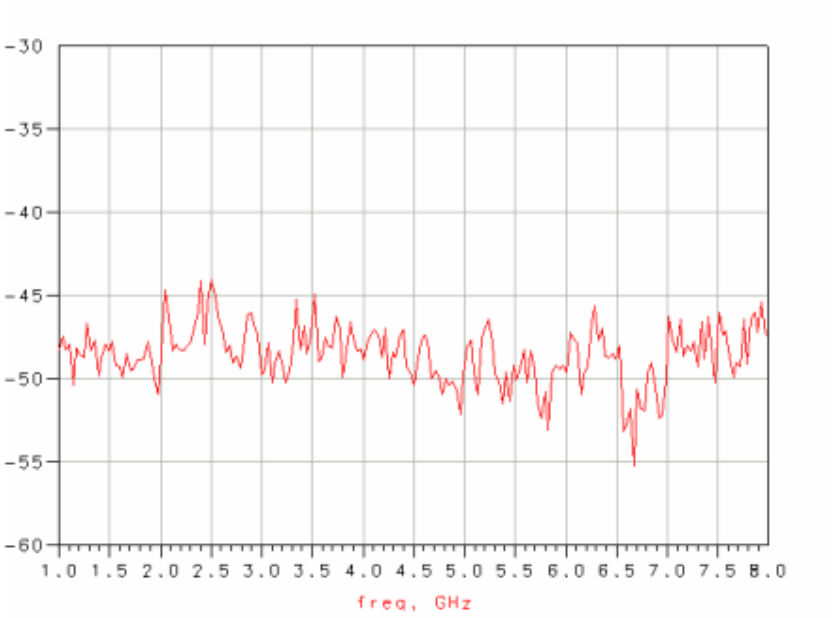

Figure (2.14) Magnitude of s11 of measured thru line not including in the standards to verifying the consistency of the standards

From figure (2.14), we could be able to confirm that the response of Through Standard is nearly -50 dB which is a reasonable for probing. Since all the results of the standards mentioned in figures reasonable, the TRL calibration is performed with this designed standards.

2.2.4 Design of Electrical Standards for measurement of the near, neighboring pins

The method used for the measurement of the near, neighboring pins of the package is implemented based on the conventional TRL calibration method. Because of the constraints of the configurations of the package as well as the measurement apparatus, the calibration kit for the multi-conductor transmission line is different from single line TRL standards.

In the designing of the calibration components of multi-conductor transmission lines, Taconic substrate with $\varepsilon_r = 10.1$, and the thickness of 62 mils is used. Detail dimensions and structures are shown in Figure (2.14). The calibration kit is designed so as to be compatible with the G-S-G air-coplanar probes and package pins. The frequency range of the calibration and the measurement is 1 GHz to 6 GHz. The calibration set consists of a zero-length Thru, a quarter wave line as a Delay, and a short as the Reflect as shown in Figure 2.15.

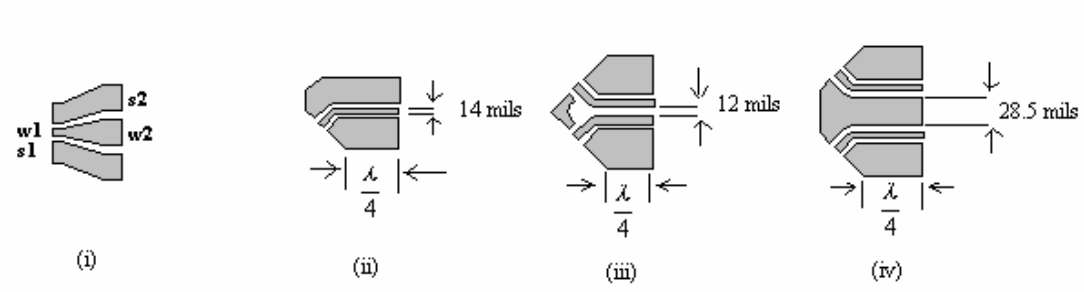

w1= width of the smaller part of theCPA

s1= witdh of the smaller slot

w2=width of the wider part of the CPA

s2= width of the wider slot

Figure (2.15) Layout of Coplanar waveguide to package adapter (CPA), interconnects enabling the measurement of the near and neighboring pins of the package. (i) CPA for the measurement of the pins of opposite ends; (ii) CPA for the measurement of the adjacent pins ; (iii) CPA for the measurement of the neighboring pins.

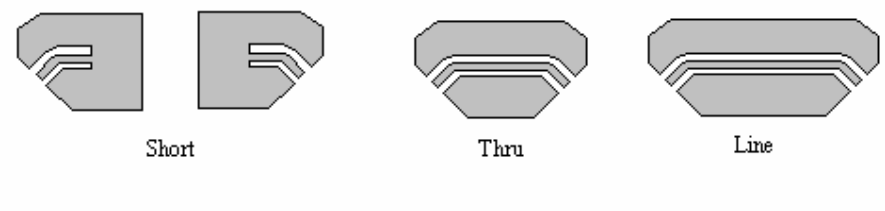

Figure (2.16) Layout of basic TRL calibration standards for the measurement of the multi-conductor line measurement.

The parameters of the calibration sets are determined and tested according to the equation (2.37) and (2.38), over the frequency range of start frequency 1 GHz to the stop frequency 6 GHz.

Electrical Length (cm)= l=2.143 cm;

Phase at 1 GHz= 25.71 Degree

Phase at 6 GHz=154.29 Degree

It is obvious that 2.143 cm line does meet the recommended insertion phase requirements between 20 and 160 degrees with respect to the THRU and it cover greater than 8:1 frequency span, so only single Line/Thru is used.

The format of the CPA traces is ground-signal-ground, which is compatible with the configuration of the air coplanar probes. The CPAs are designed as tapered structure [See Figure (2.15)] so that the proper transition between the air coplanar probes used for IC measurements. CPA are designed to be compatible with the probes which has the pitch dimension of 250 micron and the package pins which have the width of 11 mils,

and the distance between the adjacent pins is 13 mil. The length of the taper section is 20 mils in order to maintain the 50 ohm CPW structure at the transition at the probe tip.

The slot width is also designed as the tapered with connecting 2.5 mils and 5 mils. The smaller width of the taper section is 4.5mil in order to make proper transition with the probe width and the pitch of 250μ (1 mil) probe. The taper section which is designed for compatibility with the probe dimension is extended 1.5 mils further, so that the probe will be enable to probe down and sit. The larger dimension of the taper section is 14 mils and the length is also extended to quarter wavelength enabling 12 mils package pin to solder and sit properly. [Figure (2.15)]

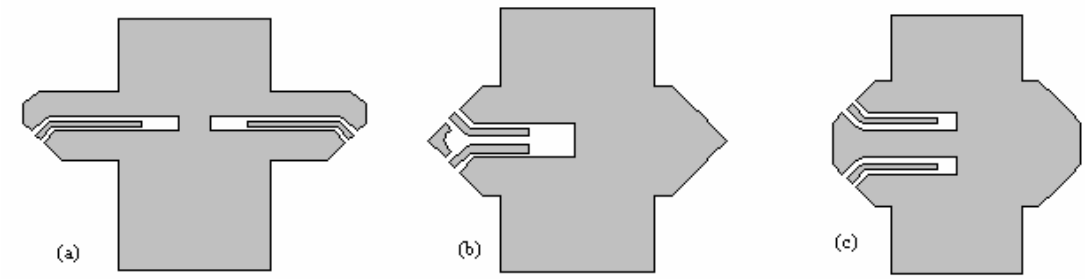

Figure (2.16) Patterns designed for package pin measurement of the set including both single lead and multi Lead.

Chapter Three

Measurement and Characterization

Having determined the structure dimensions, the material properties and the CPAs, the layouts for the calibration standards were drawn using AutoCAD. The positive, laser photo-plot masks were developed. Then, the calibration standards were developed and fabricated using the photolithography technique. (See Appendix B)

Each piece of the circuit was placed half the wavelength away from each other to avoid unnecessary coupling effects. Measurements were made with the Microtech Cascade Probe Station using air-coplanar probes in conjunction with the HP8510C Vector Network Analyzer (VNA). A Perperpex fixture was specially designed to lift the substrate up from the base plane of the probe station in order to avoid the effect of large ground plane. This is because all the interconnects were designed based on the coplanar transmission line without the ground plane.

3.1 Measurement of Single Pin

The following steps for the measurements had been performed for the single lead measurement.

(a) Step 1: Clean the surface of the circuit

(b) Step 2: Solder the package on the structure design to make proper measurements of the package

(c) Step 3: Wire bonded to the pin to be measure and the adjacent pins to the heat slug

(d) Step 4: TRL Calibration

(e) Step 5: Measure the wire bonded pins

(f) Step 6: Measure the structure alone

Figure (3.1) Microscopic view of TSSOP Lead which is mounted on the designed CPA trace.

Figure (3.1) shows the trace of epoxy which is sandwiched between package leads and the designed CPA. The A-A Line is the CPA reference plane which is the reference plane where the Leads should be properly mounted on the designed CPA with minimum reflections. The B-B Line is the probes reference plane which makes the probing of air-coplanar probes appropriately.

3.2 Measurement of Near and Neighboring Pins

The following steps for the measurements had been performed for the single lead measurement.

(a) Step 1 : Clean the surface of the circuit

(b) Step 2 : Solder the package to be measured with the conductive epoxy on the on the structure designed substrate to make proper measurements of the package

(c) Step 3 : Wire are bonded to the adjacent pins of the pin to be measured to the heat slug

(d) Step 4 : Single line TRL Calibration

(e) Step 5 : Measure the interconnects (couplers)

(f) Step 6 : Measure the desired pins

(g) Step 7 : Measure the structure alone

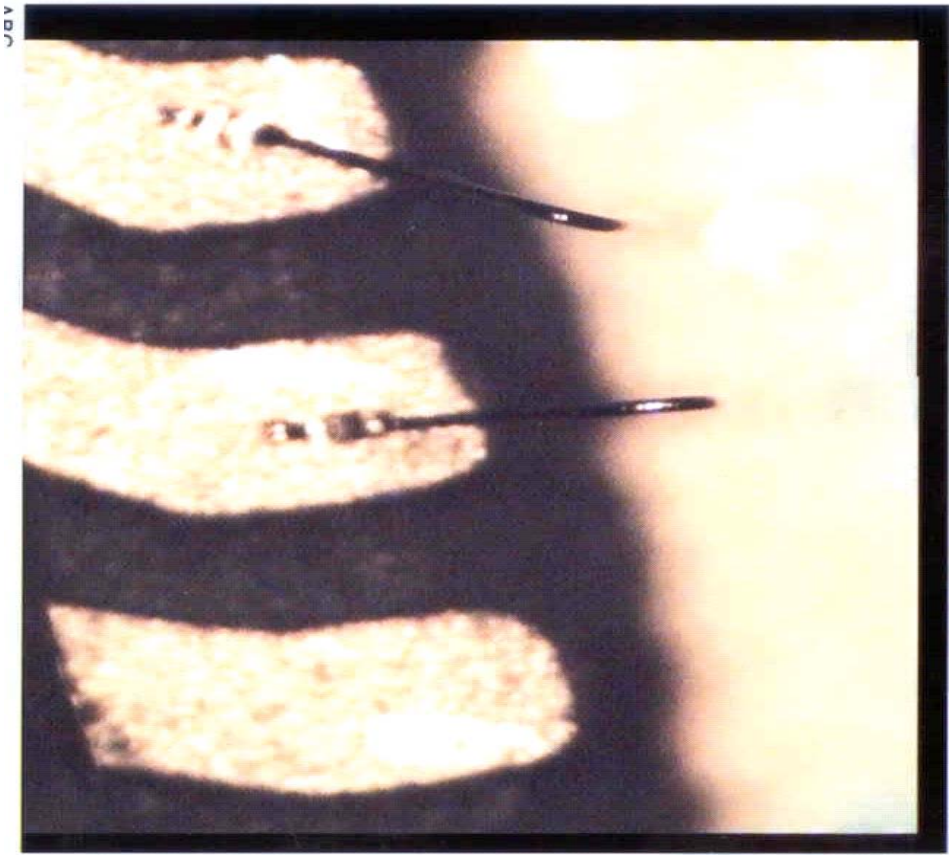

Figure (3.2) Microscopic view of outer most package lead which is wire-bonded to the heat-slug.

To measure the electrical properties of the package Leads, the package is mounted onto the Taconic wafer substrate patterned with CPA. This is designed to provide the electrical transition between the different geometry structures of air-coplanar probes and the package Lead to be measured. All possible measurement setup as well as the patterned designed and fabricated on the substrate are shown in Figure (3.3).

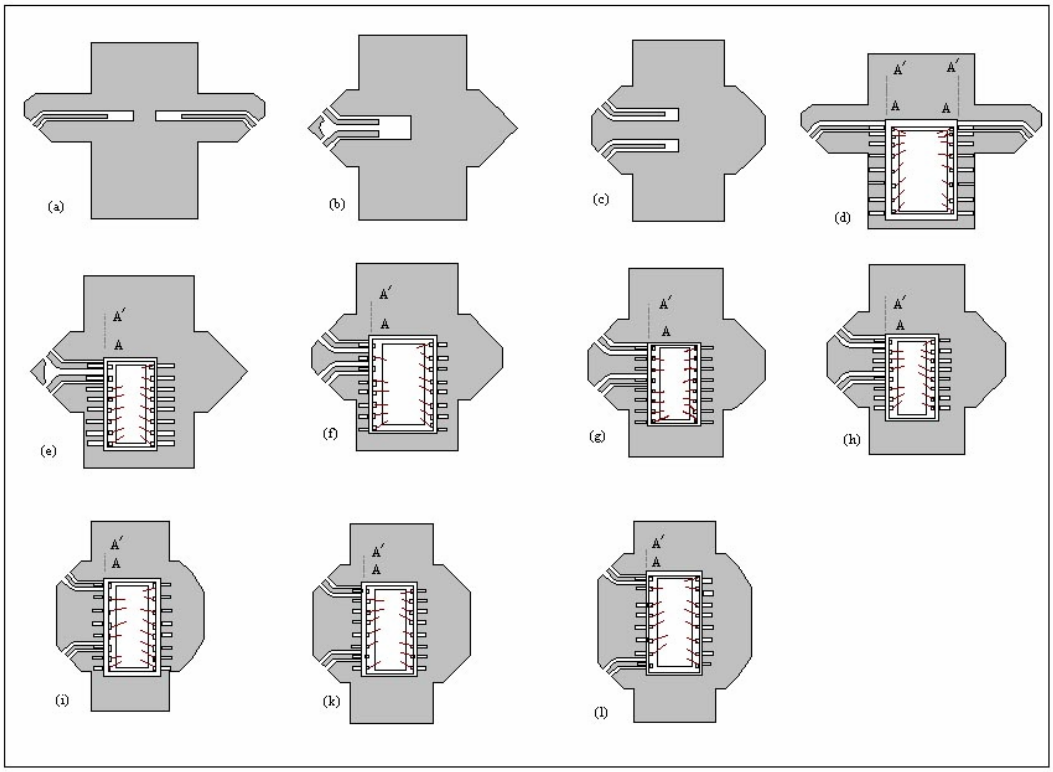

Figure (3.3) Schematic representation of the measurement setup and data collections of all possible setups.

This method, which is based on the multi-conductor lines characterization scheme [see Figure (3.3)] in conjunction with TRL calibration technique, is applied in the investigation and measurement of the electrical properties of the multi-leads plastic package. The calibration procedures and all possible data acquisitions steps are shown in Figure (3.4).

(a) Step 1 : Initial single line TRL calibrations.

(b) Step 2 : Data acquisition of Z_1 which obtained from the scattering of the interconnects for the single line characterizations.

(c) Step 3: Data acquisition of Z_1' which obtained from the scattering of the interconnects for the multi-conductor line characterizations of non-adjacent pins.

(d) Step 4 : Data acquisition of Z_1'' which obtained from the scattering of the interconnects for the multi-conductor line characterizations of adjacent pins.

The initial single line TRL calibration is performed so as to calibrate the VNA (HP 8510 C) in order to remove the imperfections of the probes and the network analyzer [Step 1 in Figure 3.4]. The first step of calibration only removes the imperfections in network analyzer and the probes. The scattering of the parameters for the pattern designed to mount the package is collected as the first step of data acquisition. [see Figure 3.5 to 3.7]

Then, the test package is subsequently soldered onto the patterned substrate using soldering cream. Separate structure with different dimensions was used for each type of pin measurements. All other pins were wire bonded to the die pad of the package, which was connected to the heat slug enabling the common grounding to the test piece. The package under test is then measured using the VNA in conjunction with the air-coplanar probes and the probe station.

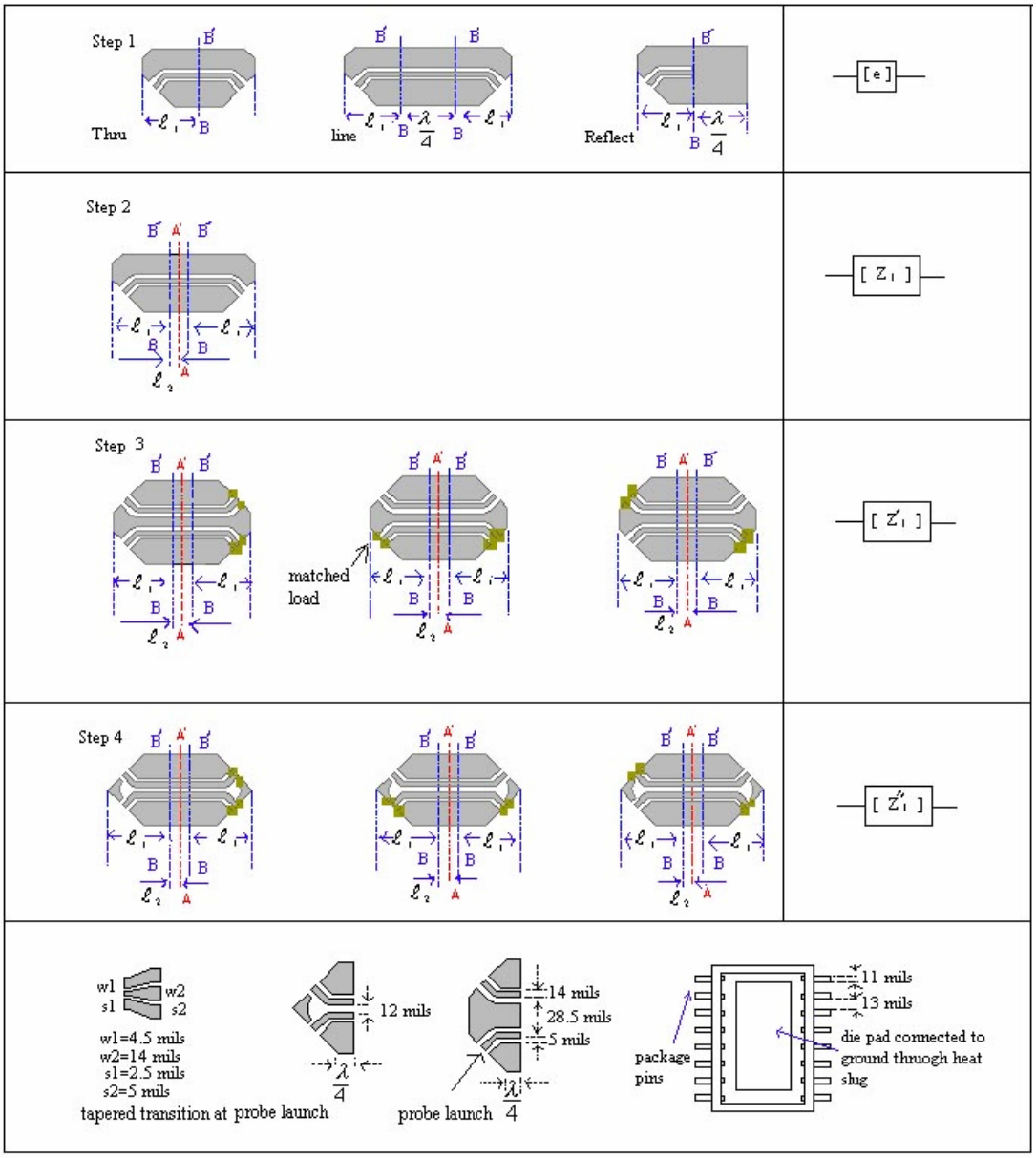

Figure (3.4) Schematic representation of the TRL calibration Set up and procedure.

In order to obtain the scattering parameters of the package only as shown in the Figure (3.8), the scattering parameters of the pattern including interconnects are de-embedded out. All the inter-couplings of the near and neighboring pins of the package are collected. The detailed procedure for de-embedding of the package parameters only are shown in the Figure [3.5 to 3.7].

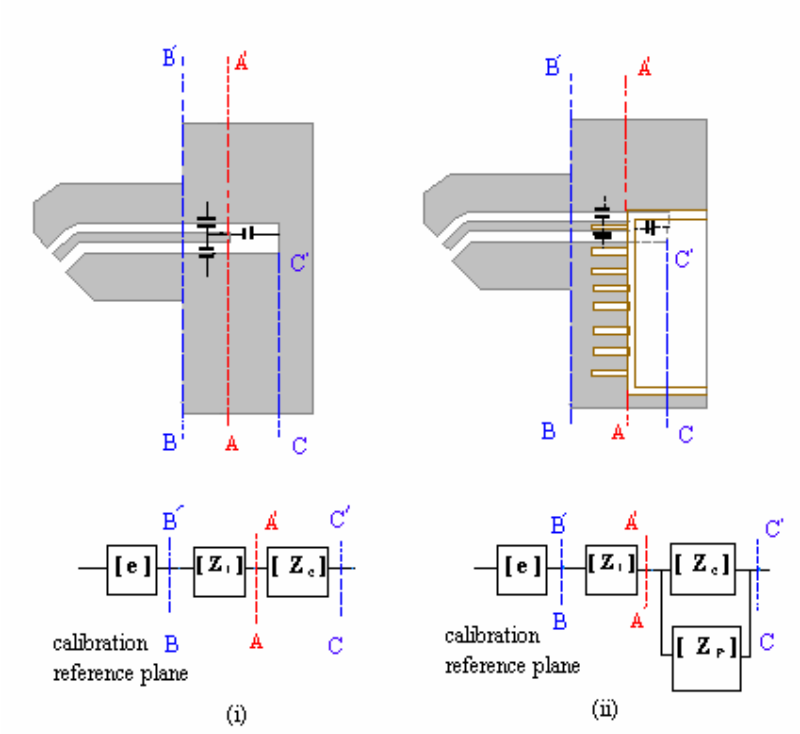

Figure (3.5) De-embedding procedure for single lead: (i) Collecting the S-parameter of the structure only; (ii) Collecting of the S-parameter of the structure with the package

As the first step, the VNA is calibrated to eliminate the error matrix [e]. The matrix can be obtained using equation (2.27) to (2.33) after the TRL calibration procedure has performed. Hence, VNA is ready to collect the desired parameters.

Then the scattering parameters of the interconnects are collected along the B-B' plane. After that, package is attached with the interconnects and the scattering parameters of the whole setup are collected, and the impedance matrix of overall $[Z_t]$, is obtained.

The relationship between the various steps are as follows:

$$[Z_1]+[Z_c]=[Z] \quad , \tag{3.1}$$

$$[Z_1]+[Z_c]//[Z_r]=[Z_t] \, ,$$

$$[Z_1]+([Y_c]+[Y_r])^{-1}=[Z_t] \tag{3.2}$$

Thus,

$$([Y_c]+[Y_r])^{-1}=[Z_t]-[Z_1],$$

$$([Z_c]^{-1}+[Z_r]^{-1})([Z_t]-[Z_1])=I,$$

$$[I]-([Z_c]^{-1}([Z_t]-[Z_1]))=[Z_r]^{-1}([Z_t]-[Z_1])$$

$[Z_r]$ can be derived.

$$[Z_r]=([Z_t]-[Z_1])([I]-([Z_c]^{-1}([Z_t]-[Z_1])))^{-1} \, . \tag{3.3}$$

From Figure (3.4) step 2, $[Z_1]$ was determined and $[Z_c]$ can be simply obtained by subtracting the impedance matrix of the interconnects from the overall measured impedance .

$$[Z_c]=[Z]-[Z_1]$$

The impedance matrix of package is easily extracted by using equations (3.2) and (3.4). From Figure 3.5 the following equations are obtained.

$$Z_{r1}\,]= [Z_c]+ [Z_r\,] \tag{3.5}$$

$$[Z_t\,]= [Z_1]+ [Z_c] \tag{3.6}$$

$$[Z_r]= (\,[\,Z_t]- [Z_1])(\,[I]- ([Z_c]^{-1}([\,Z_t]- [Z_1])))^{-1}\ . \tag{3.7}$$

The data acquired by measurements are extracted by the equations (3.7) by using Matlab. Then, scattering of the package is extracted using $[Z_r\,]$ in the MDS , EM simulator and solver. The acquired data is used to determined the parasitic of the package, which plays important part in the electronic packaging industry.

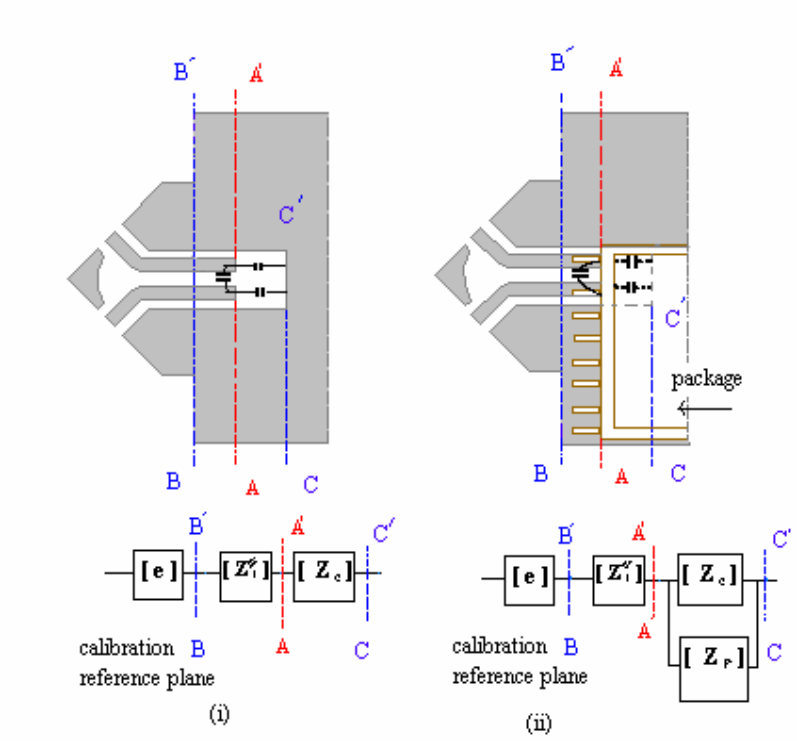

Figure (3.6) De-embedding procedure for adjacent leads: (i) Collecting the S-parameter of the structure only; (ii) Collecting of the S-parameter of the structure with the package

Similarly, from figure 3.6, we get the equations as

$$[Z_1''] + [Z_c] = [Z'']$$ (3.8)

$$[Z_1''] + [Z_c] // [Z_r] = [Z_t'']$$ (3.9)

Hence, $[Z_r] = ([Z_t] - [Z_1''])([I] - ([Z_c]^{-1}([Z_t] - [Z_1''])))^{-1}$ (3.10)

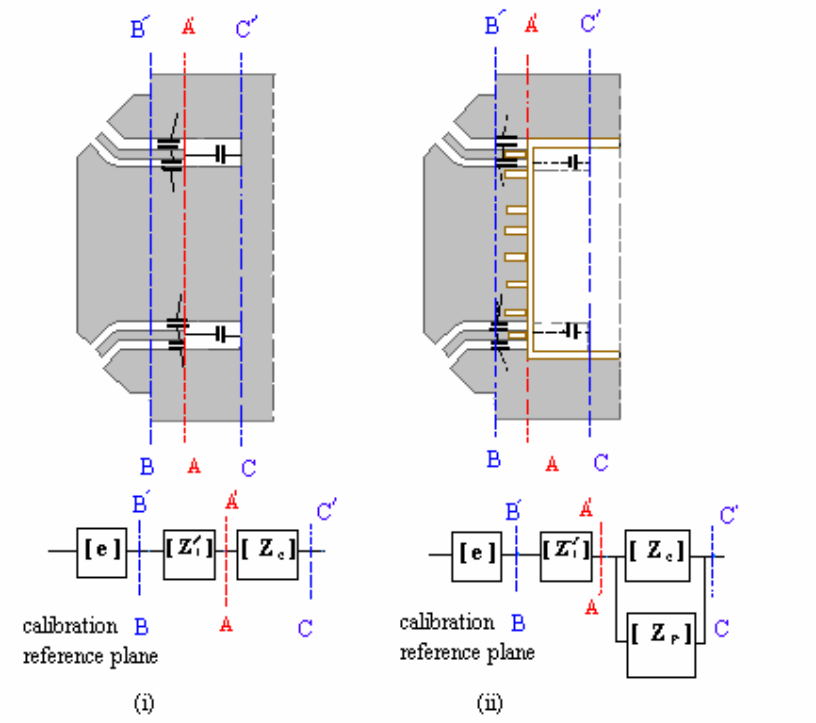

Figure (3.7) De-embedding procedure for neighboring leads: (i) Collecting the S-parameter of the structure only; (ii) Collecting of the S-parameter of the structure with the package

Similarly, from Figure(3.7), the package impedance can be obtained.

$$[Z_r]= ([Z_t]- [[Z_1^{'}]])([I]- ([Z_c]^{-1}([Z_t]- [[Z_1^{'}]])))^{-1} \qquad (3.11)$$

The procedure of the data collection is shown in the Figure 3.8.

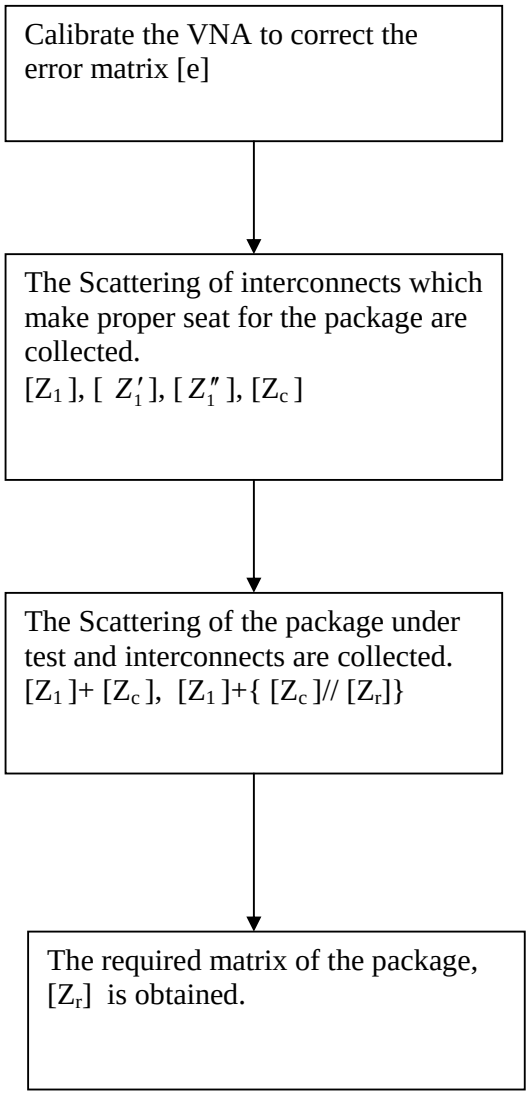

Figure (3.8) Flowchart diagram of the procedures in obtaining the required scattering matrix of the package.

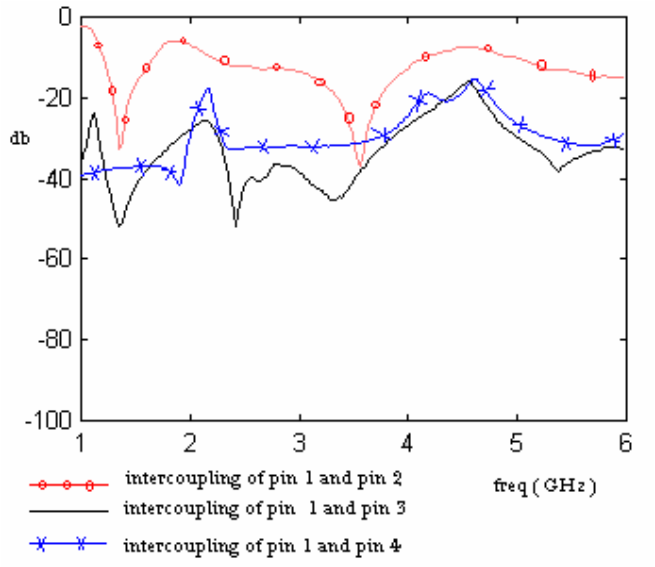

Figure (3.9) Measured inter-couplings of Near and Neighboring Pins

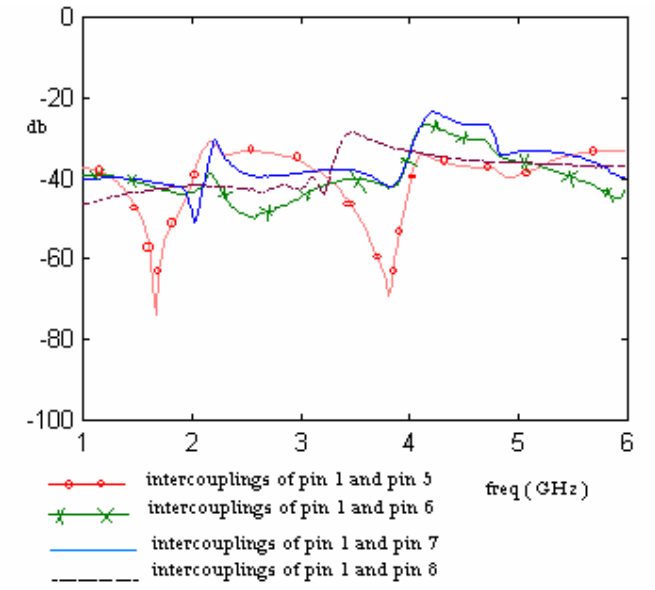

Figure (3.10) Measured inter-couplings of Near and Neighboring Pins

Figure (3.9) and (3.10) shows the plot of the inter-coupling of Leads at the single side with the reference Lead, Lead 1. Since, it is assumed that the package is symmetric, measurement is only done at the one side of the package, while considering inter-couplings of the near and neighboring pins. From the Figures, one obviously noted that the intercoupling of the adjacent pins is the strongest, while that of the reference Lead and the Lead 8 is the lowest. As a result, they can be neglected. The data obtained from measurements are calculated and then imported to the MDS Simulator to extract the lump element and transmission line model.

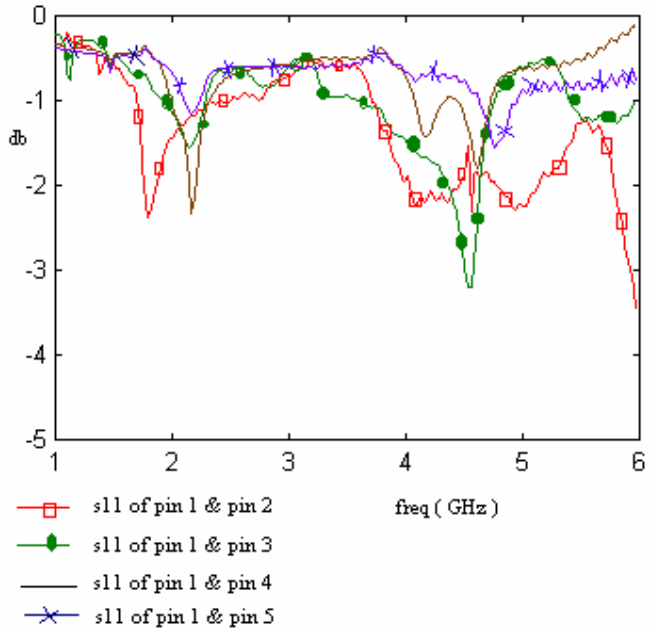

Figure (3.11) Measured s11 of more nearer package pins

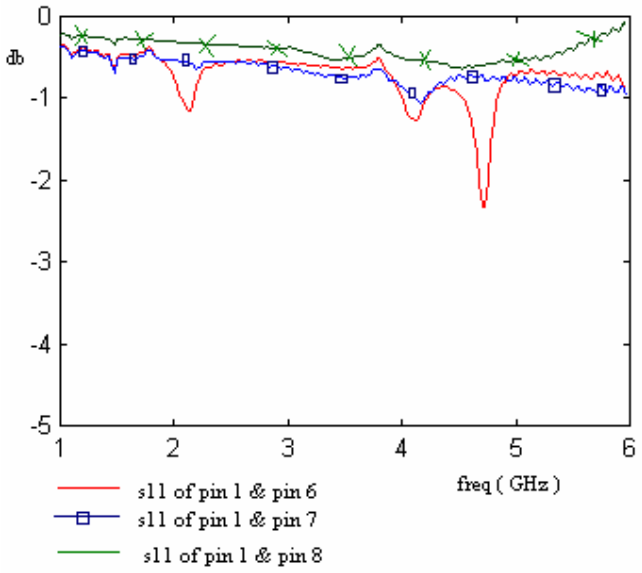

Figure (3.12) Measured s11 of package pins

Figure (3.11) and (3.12) represent the curves S11 of Leads with reference to the reference lead, Lead 1. The comparison of the graph in Figure (3.11) and (3.12) shows that the couplings between Lead 1 and Lead 2 to Lead 1 and Lead 5 have strong effect on the S11 while the couplings of Lead 1 and Lead 6 to Lead 1 and Lead 8 have less effect on the S11, while measuring the package. The data are collected and imported to IE3D and extracted in the curves shown the figures.

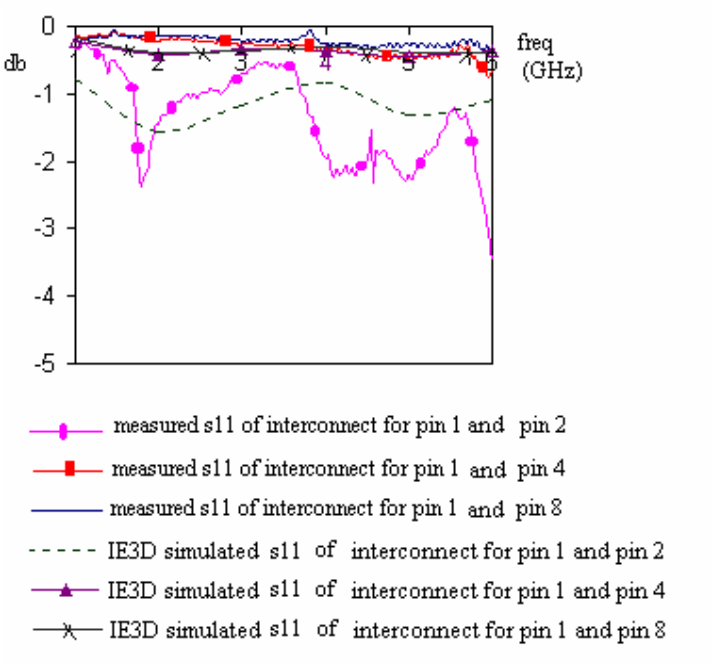

Figure (3.13) Comparison of Measured and Simulated Scattering of Interconnects

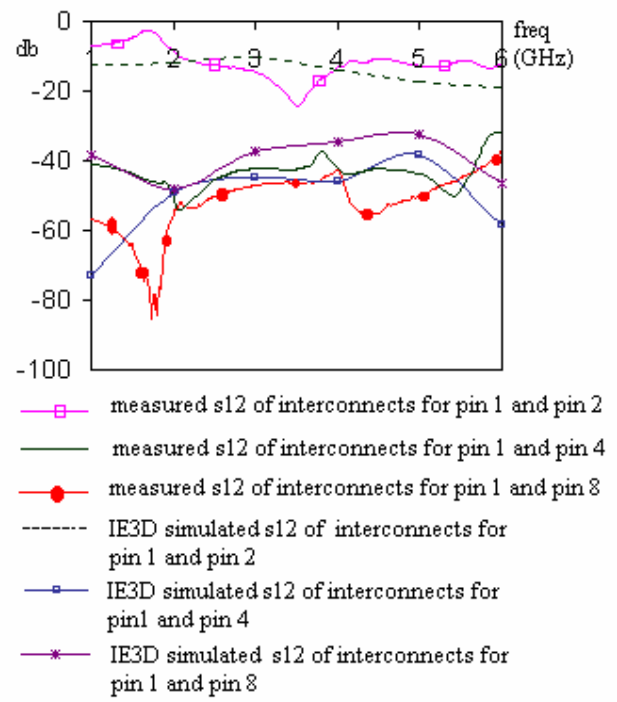

Figure (3.14) Comparison of Measured and Simulated Scattering of Interconnects

According to Figure 3.13 and 3.14, the comparison of the Measured and Simulated Scattering of interconnects (S11) and (S12) respectively are more in agreement for the far-end leads such as Lead 1 and Lead 4 as well as Lead 1 and Lead 8. While looking to the results of Lead 1 and Lead 2, which are the nearest neighbors, the measured results are some extent differed from the simulated. We can conclude that the coupling is stronger and more disturbing when the transmissions are nearer. Thus, considering the usage of pin in IC circuits, the choice of the usage of the pin is very important. The data acquired from the experiment are imported to MDS and the modeling of the Lead under test will be carried out in next chapter.

Chapter 4

Modelling

From the collected data from the measurements discussed in Chapter 3, the electrical characterization was carried out by both the lump element modeling and transmission line modeling method. Using the acquired data, the electrical element circuit parameters were optimized using MDS (Microwave Design System).

4.1 Lump Element Modeling

A common approach to characterize the line is to model the characteristics using lumped circuit elements that represent small sections of the line. Each section is supposed to be electrically short at the highest frequency of interest.

Firstly, for the lump element modeling, a model of single lead was derived. The basic elements that represented the transmission line were used to represent the individual pin. With the data collected, the model is optimized using HP-MDS optimizer.

4.1.1 Lump Element Modeling Without Coupling

The lump element circuit topology is chosen depending on the basic transmission line representing theory realizing that the individual lead exhibits a transmission line behavior. The general single transmission line representation is as follows.

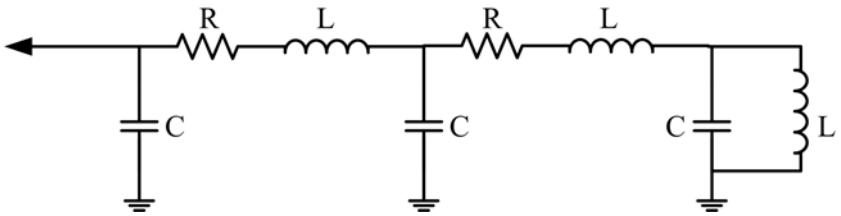

Figure (4.1) General circuit topology for the wire-bond terminated single lead configuration

For this model, the analytical formula in equation (4.1) [36] for Lead Inductance is used to estimate the initial Lead inductance in optimizing where the Lead data could be referenced from Table (1.1).

$$L_{self} = 51\ [\ln(\frac{2l}{w+t}) + 0.5]\ , \qquad (4.1)$$

Where, l= Lead Length

w= Lead Width

t= Lead Thickness

This model topology for single lead was simplified by neglecting the effects of the mutual couplings between the non adjacent pins. The configuration and the structure of G-S-G probes approximated the transmission line feed, so the mutual inductance from the signal Lead to the grounded Lead at each side was assumed to be negligible. The first part of the set of resistor and inductor represented the portion of the L3 in Figure 1.1 (b) and first two capacitors represented the capacitance at the open end input part of the lead and the capacitance at the band portion of the lead respectively. The second set of the resistor and the inductor represents the portion of L1 of Figure 1.1 (b).

The basic model was modified by adding resistors in series with the capacitor at the input side of the pin and with the inductor at the shorted end shown in Figure (4.2).

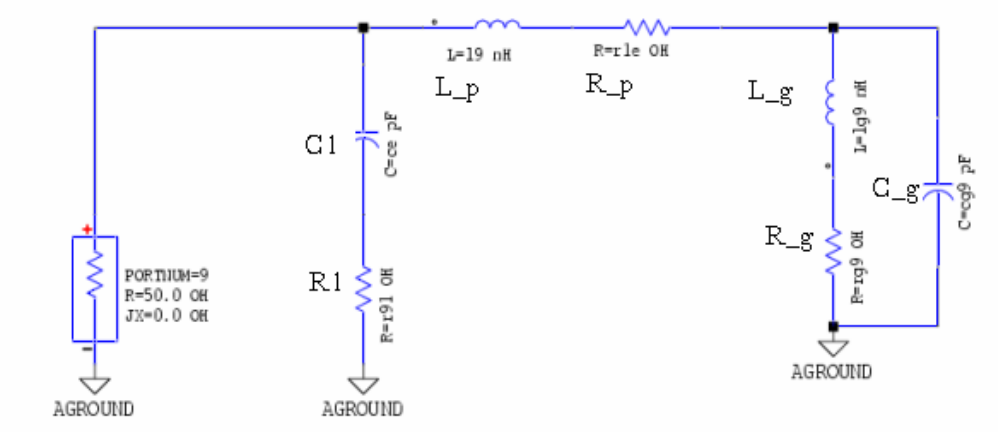

Figure (4.2) Modified circuit topology for the wire-bond terminated single lead configuration

4.12 Lump Element Modeling with Coupling

Lump element Modeling with coupling is generally refer to as the considering the effect of the near and neighboring pins of the package. This model topology for multi lead was chosen to simplify by counting the effects of the mutual couplings between inductance lead and capacitance between the non adjacent pins. The configuration and the structure of G-S-G probes approximated.

So the mutual inductance from the signal pin to the grounded pins at each side was considered. Then the sets of mutual coupling between the Pin1-Pin2, Pin1-Pin3, Pin1-Pin4 are extracted using the Network Analyzer and optimized using MDS. And the resulted obtained are shown in the tables in this Chapter.

The individual results are shown and the important procedures of derivation of Flux and the accuracy determination process in fabricating interconnects, photolithography technology, are described at the end of this chapter.

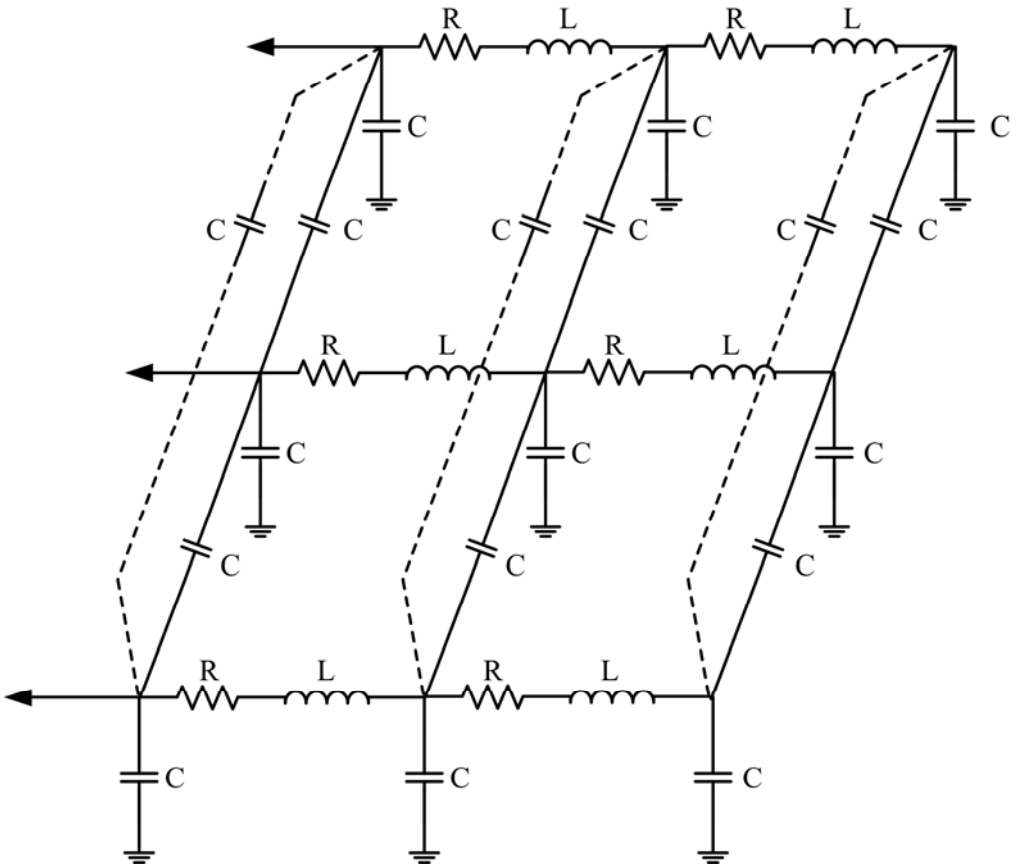

Figure (4.3) General circuit topology for the open-ended termination of adjacent leads (2 pins) configuration

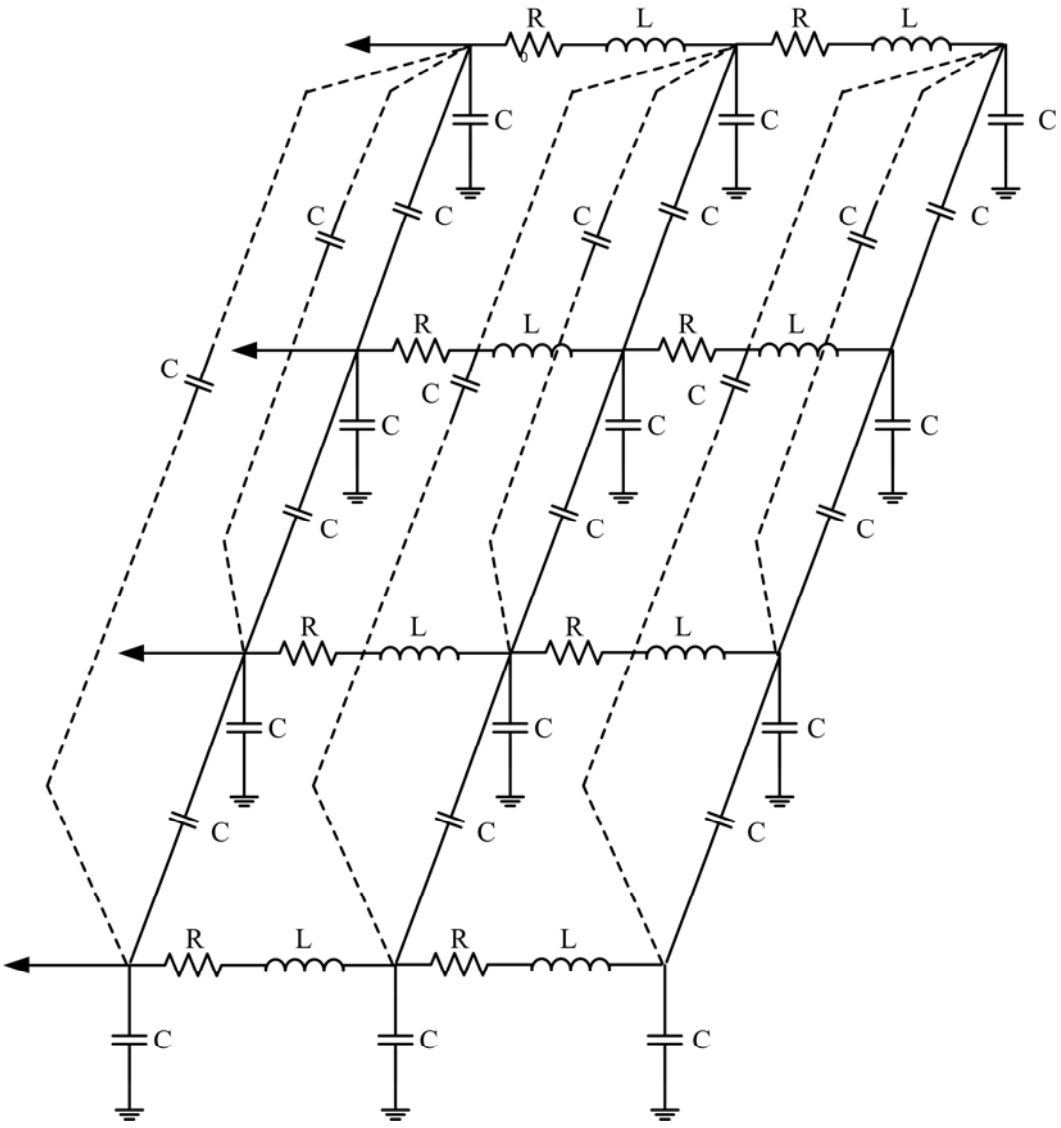

Figure (4.4) General circuit topology for the open-ended termination of four adjacent leads (4 pins) configuration.

Figure (4.3) & Figure (4.4) show the circuit topology for the open termination which is reflect termination of three and four consecutive Leads of the package under test, respectively. The capacitance in the model is to account for the couplings between adjacent pins, the couplings between next adjacent pins which are the couplings between Pin 1 and Pin 3 as well as couplings between Pin 1 and Pin 4.

The considered topology is modified of basic structure in general determination of a transmission line. And the circuit is modified in figures shown in Table 4.2.

The length of Lead is represented by a resistor and an inductor as lump elements. The ground capacitance at each node is also accounted for. This model is used in determination of the lumped element values of multi-conductor leads in MDS Optimizer. The results are shown in Table (4.1) and (4.2).

L- pin (nH)	Inter-coupling (pF)	C-g (pF)
0.9	0.6	0.089

Table(4.1) The extracted electrical parameters of the lumped element modeling without coupling between near and neighboring pins.

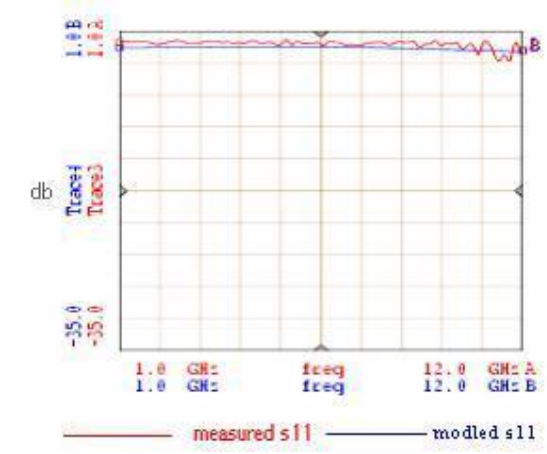

Figure (4.5) The Comparison of the simulated and modeled S11 and S12

	C1 (pF)	R1 (kΩ)	L_p (nH)	R_p (Ω)	Cpi (pF)	Cp (pF)	L_g (nH)	R_g (Ω)	C_g (pF)
Pin1	0.069	0.9	0.91	1.7	1E-11	0.060	0.100	0.79	0.026
Pin2	0.030	0.88	0.84	1.9	1E-11	0.061	0.210	0.76	0.011
Pin3	0.089	0.89	0.9	1.8	1E-11	0.050	0.128	0.72	0.011
Pin4	0.053	0.83	0.56	1.1		0.057	0.060	0.73	0.022
Pin13	0.066	0.80	1.0	1.63	1E-11	0.063	0.070	0.69	0.014
Pin14	0.067	0.912	0.9	1.9	1E-11	0.06	0.066	0.72	0.012
Pin15	0.04	0.95	0.75	1.5	1E-11	0.05	0.050	0.72	0.012
Pin16	0.08	0.9	0.6	2.0		0.05	0.061	0.8	0.010

Cpi=inter-coupling between non adjacent pins(pin 1 and pin 3)

Cp= inter-coupling between adjacent pins

Table (4.2) lump element values of the package parasitic and bond wire

The Lump element values of the Leads are collected in Table (4.1) and (4.2) in the reference of figure 4.1 and 4.2. C1 in Table (4.1) is the capacitance between the ground and the Lead. C_g is the bond wire capacitance and Cp and Cpi are intercouplings of adjacent pins and non adjacent pins, respectively.

4.2 Transmission Line Modelling

Pin	Capacitance (pF)	Length of Line (mil)
1	0.16	20.5
2	0.17	20.7
3	0.13	25.4
4	0.14	22.3

ε_r = 9.6 , Characteristic Impedance= 489.5 Ω ;

Mutual Coupling between adjacent lines=0.12 pF.

Table (4.3) Transmission lines values of the package parasitic and bond wire

MDS optimizer is used to predict the transmission line model of the package leads with the data acquired form the measurement. Thus the permittivity, ε_r is 9.6 . The couplings between lines is optimized as 0.12 pF . The detailed results are shown in Table 4.3.

4.3 Formulation of the Lead Parasitics

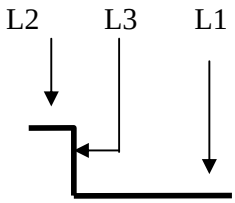

Figure (4.6) General configuration of package lead

The concept of partial inductance is used to describe the lumped inductances originating from parasitic effects of the package.

Each segment is considered to be a straight conductive element with a triangle wave current directed parallel to the length and has negligible cross-section. For a given current distribution for each segment, which has unique current direction, the magnetic vector potential, $\overline{A}$, is in the direction of that current.

The current and the magnetic vector potential on each segment are respectively given as:

For segment 1

$$\bar{I} = \overline{I_x} = \hat{x} I_o \times \frac{2}{L_1} \times \frac{EXP(-jkR)}{R} \begin{cases} x & ,0 \le x \le \frac{L_1}{2}, \\ -(x - L_1), & \frac{L_1}{2} \le x \le L_1, \end{cases} \tag{4.2}$$

For segment 2

$$\bar{I} = \overline{I_z} = \hat{z} I_o \times \frac{2}{L_2} \times \frac{EXP(-jkR)}{R} \begin{cases} -z & ,0 \le z \le \frac{L_2}{2}, \\ (z - L_2), & \frac{L_2}{2} \le z \le L_2, \end{cases} \tag{4.3}$$

For segment 3

$$\bar{I} = \overline{I_x} = \hat{x} I_o \times \frac{2}{L_3} \times \frac{EXP(-jkR)}{R} \begin{cases} -x & ,0 \le x \le \frac{L_3}{2}, \\ (x + L_3), & \frac{L_3}{2} \le x \le L_3, \end{cases} \tag{4.4}$$

$R = \sqrt{x^2 + y^2 + z^2}$,

For segment 1,the magnetic vector potential $\overline{A1}$ is

$$\overline{A1} = \hat{x}\frac{\mu_o}{4\pi}\frac{EXP(-jkR)}{R} I_o \times \frac{2}{L_1} \times [\int_0^{l_1/2}(x)dx - \int_{L_1/2}^{L_1}(x - L_1)dx]$$

$$= \hat{x}\frac{\mu_o}{4\pi}\frac{EXP(-jkR)}{R} I_o \times \frac{2}{L_1} \times [(\frac{x^2}{2})_0^{L_1/2} - [(\frac{x^2}{2} - L_1 x)]_{L1/2}^{L_1}]$$

$$= \hat{x}\frac{\mu_o}{4\pi}\frac{EXP(-jkR)}{R} I_o \times \frac{2}{L_1} \times [(\frac{{L_1}^2}{8}) - [(\frac{{L_1}^2}{2} - {L_1}^2) - (\frac{{L_1}^2}{8} - \frac{{L_1}^2}{2})]$$

$$= \hat{x}\frac{\mu_o}{4\pi}\frac{EXP(-jkR)}{R} I_o \times \frac{L_1}{2}, \qquad (4.5)$$

For segment 2,the magnetic vector potential $\overline{A2}$ is

$$\overline{A2} = \hat{z}\frac{\mu_o}{4\pi}\frac{EXP(-jkR)}{R}I_o \times \frac{2}{L_2} \times [\int_0^{L_2/2}(-z)dz + \int_{L_2/2}^{L_2}(z-L_2)dz]$$

$$= \hat{z}\frac{\mu_o}{4\pi}\frac{EXP(-jkR)}{R}I_o \times \frac{2}{L_2} \times [-(\frac{z^2}{2})_0^{L_2/2} + [(\frac{z^2}{2} - L_2 z)]_{L_2/2}^{L_2}]$$

$$= \hat{z}\frac{\mu_o}{4\pi}\frac{EXP(-jkR)}{R}I_o \times \frac{2}{L_2} \times [-(\frac{{L_2}^2}{8}) + [(\frac{{L_2}^2}{2} - {L_2}^2) - (\frac{{L_2}^2}{8} - \frac{{L_2}^2}{2})]$$

$$= -\hat{z}\frac{\mu_o}{4\pi}\frac{EXP(-jkR)}{R}I_o \times \frac{L_2}{2}, \qquad (4.6)$$

For segment 3,the magnetic vector potential $\overline{A3}$ is

$$\overline{A3} = \hat{x}\frac{\mu_o}{4\pi}\frac{EXP(-jkR)}{R}I_o \times \frac{2}{L_3} \times [-\int_0^{-L_3/2}(x)dx + \int_{-L_3/2}^{-L_3}(x+L_3)dx]$$

$$= \hat{x}\frac{\mu_o}{4\pi}\frac{EXP(-jkR)}{R}I_o \times \frac{2}{L_3} \times [-(\frac{x^2}{2})_0^{-L_3/2} + [(\frac{x^2}{2} + L_3 x)]_{-L_3/2}^{-L_3}$$

$$= \hat{x}\frac{\mu_o}{4\pi}\frac{EXP(-jkR)}{R}I_o \times \frac{2}{L_3} \times [-(\frac{{L_3}^2}{8}) + [(\frac{{L_3}^2}{2} - {L_3}^2) - (\frac{{L_3}^2}{8} - \frac{{L_3}^2}{2})]]$$

$$= -\hat{x}\frac{\mu_o}{4\pi}\frac{EXP(-jkR)}{R}I_o \times \frac{L_3}{2} \qquad (4.7)$$

The magnetic field intensity $\overline{H}$, is defined as

$$\overline{H} = \frac{1}{\mu_o}(\nabla \times \overline{A}) \tag{4.8}$$

$$\nabla \times \overline{A} = \left[\hat{x}\left(\frac{\partial A_z}{\partial y} - \frac{\partial A_y}{\partial z} \right) + \hat{y}\left(\frac{\partial A_x}{\partial z} - \frac{\partial A_z}{\partial x} \right) + \hat{z}\left(\frac{\partial A_y}{\partial x} - \frac{\partial A_x}{\partial y} \right) \right] \tag{4.9}$$

In free space, the magnetic flux density is $\overline{B}$, is defined as

$$\overline{B} = \mu_o \times \overline{H} \tag{4.10}$$

where $\overline{B}$ is in webers per square meter and μ_o is the free space permeability.

The flux Φ passing through the area S, is defined as

$$\Phi = \int_s \overline{B} \cdot d\overline{S} \tag{4.11}$$

For segment 1, the magnetic field intensity $\overline{H1}$ is

$$\overline{H1} = \frac{I_o}{4\pi} \times \left[\hat{y}\left(\frac{\partial Ax}{\partial z}\right) - \hat{z}\left(\frac{\partial Ax}{\partial y} \right) \right]$$

$$= \begin{aligned} & -\frac{I_o}{4\pi} \times \left[\hat{y}\left\{ \frac{EXP(-jk\sqrt{x^2+y^2+z^2})}{(x^2+y^2+z^2)^{3/2}} + j\frac{EXP(-jk\sqrt{x^2+y^2+z^2})}{x^2+y^2+z^2}k \right\} z \right. \\ & \left. + \hat{z}\left\{ \frac{EXP(-jk\sqrt{x^2+y^2+z^2})}{(x^2+y^2+z^2)^{3/2}} + j\frac{EXP(-jk\sqrt{x^2+y^2+z^2})}{(x^2+y^2+z^2)}k \right\} y \right] \times \frac{L_1}{2}. \end{aligned} \tag{4.12}$$

$$\overline{B1} = -\frac{\mu_o I_o}{4\pi}\times\left[\hat{y}\left\{\frac{EXP(-jk\sqrt{x^2+y^2+z^2})}{(x^2+y^2+z^2)^{3/2}}+j\frac{EXP(-jk\sqrt{x^2+y^2+z^2})}{x^2+y^2+z^2}k\right\}z + \hat{z}\left\{\frac{EXP(-jk\sqrt{x^2+y^2+z^2})}{(x^2+y^2+z^2)^{3/2}}+j\frac{EXP(-jk\sqrt{x^2+y^2+z^2})}{(x^2+y^2+z^2)}k\right\}y\right]\times\frac{L_1}{2}$$

$$= -\frac{\mu_o I_o}{4\pi}\times\frac{L_1}{2}\times\frac{EXP(-jkR)}{R^2}\times\left(\frac{1}{R}+jk\right)\times\left[(\hat{y}\times z)+(\hat{z}\times y)\right], \quad (4.13)$$

Flux passing through surface of the segment 1,

$$\Phi_1 = \int_0^{L_1}\int_0^{w}\overline{B1}\cdot d\overline{S}$$

$$= \frac{\mu_o I_o}{4\pi}\times\frac{L_1}{2}\times\int_0^{L_1}\int_0^{w}\left[(\frac{EXP(-jkR)}{R^2}\times(\frac{1}{R}+jk))\times\{\left[(\hat{y}z)+(\hat{z}y)\right]\cdot\hat{z}(dxdy)\}\right]$$

$$= \frac{\mu_o I_o}{4\pi}\times\frac{L_1}{2}\times\int_0^{L_1}\int_0^{w}\left[(\frac{EXP(-jkR)}{R^2}\times(\frac{1}{R}+jk))\times\{\left[(\hat{y}z)+(\hat{z}y)\right]\cdot\hat{z}(dxdy)\}\right], \quad (4.14)$$

From Biot-Savart Law,

$$\Phi_1 = l_1 I_1, \quad (4.15)$$

Thus, we get,

$$l_1 = \frac{\Phi_1}{I_1}, \quad (4.16)$$

where l_1 is the inductance of the first section of lead where the length of L3 and L2 are very much smaller than L1 from the measured data and the whole lead could be counted as L1.

Since, LC= $\mu\varepsilon$, (4.17)

$$C= \frac{\mu\varepsilon}{L} = \frac{\mu\varepsilon}{l_1} = \frac{\mu\varepsilon I_1}{\Phi_1}, \tag{4.18}$$

$$C= \mu\varepsilon I_1 \Big/ \{ \frac{\mu_o I_o}{4\pi} \times \frac{L_1}{2} \times \int_0^{L_1}\int_0^{w} \Big[(\frac{EXP(-jkR)}{R^2}(\frac{1}{R}+jk))\{[(\hat{y}z)+(\hat{z}y)]\cdot \hat{z}(dxdy)\} \Big] \} \tag{4.19}$$

$$C = \mu\varepsilon I_1 \Big/ \{\frac{\mu_o I_o}{4\pi}\frac{L_1}{2}\int_0^{L_1}\int_0^{w}(\frac{EXP(-jkR)}{R^2}(\frac{1}{R}+jk)y(dxdy)\} \tag{4.20}$$

$$L=\{ \frac{\mu_o I_o}{4\pi}\frac{L_1}{2}\int_0^{L_1}\int_0^{w}\Big[(\frac{EXP(-jkR)}{R^2}(\frac{1}{R}+jk))y(dxdy)\Big]\} \Big/ I_1 \tag{4.21}$$

To get parasitics by per unit length and forcing $I_o = I_1$,

Self Inductance of each segments can be obtained :

$$L_{self}= \frac{2\mu_o}{\pi} \Big(0.25 \Big[\frac{1}{w}S(\frac{w}{\alpha_i})+\frac{1}{t}S(\frac{t}{\alpha_w})+S(\frac{1}{r}) \Big]$$

$$+ \frac{1}{24}\Big[\frac{t^2}{w}S\Big(\frac{w}{t\alpha_1(r+\alpha_r)}\Big)+\frac{w^2}{t}S\Big(\frac{t}{w\alpha_w(r+\alpha_r)}\Big)$$

$$+\frac{t^2}{w^2}S\left(\frac{w^2}{tr(\alpha_i+\alpha_r)}\right)+\frac{w^2}{t^2}S\left(\frac{t^2}{wr(\alpha_w+\alpha_r)}\right)$$

$$+\frac{1}{wt^2}S\left(\frac{wt^2}{\alpha_1(\alpha_w+\alpha_r)}\right)+\quad\frac{1}{tw^2}S\left(\frac{tw^2}{wr(\alpha_i+\alpha_r)}\right)\Bigg]$$

$$-\frac{1}{6}\left[\frac{1}{wt}T\left(\frac{wt}{\alpha_r}\right)+\frac{t}{w}T\left(\frac{w}{t\alpha_r}\right)+\frac{w}{t}T\left(\frac{t}{w\alpha_r}\right)\right]$$

$$-\frac{1}{60}\Bigg[\frac{(\alpha_r+r+t+\alpha_i)t^2}{(\alpha_r+r)(r+t)(t+\alpha_i)(\alpha_r+\alpha_i)}$$

$$+\frac{(\alpha_r+r+w+\alpha_w)w^2}{(\alpha_r+r)(r+w)(w+\alpha_w)(\alpha_r+\alpha_i)}+\frac{(\alpha_r+\alpha_w+1+\alpha_i)}{(\alpha_r+\alpha_w)(\alpha_w+1)(1+\alpha_i)(\alpha_r+\alpha_i)}\Bigg]$$

$$-\frac{1}{20}\left[\frac{1}{r+\alpha_r}+\frac{1}{\alpha_w+\alpha_r}+\frac{1}{\alpha_i+\alpha_r}\right]\Bigg) \tag{4.21}$$

Where w=$\frac{w}{l}$, t=$\frac{T}{l}$,r=$\sqrt{w^2+t^2}$, $\alpha_w=\sqrt{w^2+1}$, $\alpha_i=\sqrt{t^2+1}$, $\alpha_w=\sqrt{w^2+t^2+1}$,

S(X)=$\sinh^{-1}$(X)=ln(x+$\sqrt{1+x^2}$), T(X)=$\tan^{-1}$(X).

w= width of the conductor, t= thickness of the conductor, l= length of individual segments of the Lead.

Thus, the Mutual Inductance can be calculated as

$$M_{ij}=\frac{0.001}{w_1w_2t_1t_2}\Bigg[\Bigg[\Bigg[\left(\frac{y^2z^2}{4}-\frac{y^4}{24}-\frac{z^4}{24}\right).x.\ln\left(\frac{x+\sqrt{x^2+y^2+z^2}}{\sqrt{y^2+z^2}}\right)$$

$$+\left(\frac{z^2x^2}{4}-\frac{x^4}{24}-\frac{z^4}{24}\right).y.\ln\left(\frac{y+\sqrt{x^2+y^2+z^2}}{\sqrt{x^2+z^2}}\right)$$

$$+\left(\frac{y^2x^2}{4}-\frac{x^4}{24}-\frac{y^4}{24}\right).z.\ln\left(\frac{z+\sqrt{x^2+y^2+z^2}}{\sqrt{y^2+x^2}}\right)$$

$$+\frac{1}{60}(x^4+y^4+z^4-3x^2y^2-3y^2z^2-3z^2x^2)\sqrt{x^2+y^2+z^2}$$

$$-\frac{xyz^3}{6}\tan^{-1}\left(\frac{xy}{x\sqrt{x^2+y^2+z^2}}\right)-\frac{xy^3z}{6}\tan^{-1}\left(\frac{xz}{y\sqrt{x^2+y^2+z^2}}\right)$$

$$-\frac{x^3yz}{6}\tan^{-1}\left(\frac{zy}{x\sqrt{x^2+y^2+z^2}}\right)\Bigg]_{D_y+w_2-w_1,D_y}^{Dy\,w1,Dy+w2}(x)\Bigg]_{D_x+t_2-t_1,D_x}^{D_x-t_1,D_x+t_2}(y)\Bigg]_{Dz+l_2-l_1,Dz}^{Dz-l_{11},D_x+l_2}(z) \quad (4.22)$$

Where $[[[f(x,y,z)]_{q2,q4}^{q1,q3}(x)]_{r2,r4}^{r1,r3}(y)]_{s2,s4}^{s1,s3}(z)=\sum_{i=1}^{4}\sum_{j=1}^{4}\sum_{k=1}^{4}(-1)^{i+j+k+1}.f(q_i+r_j+s_k)$

The required L and C of the package leads are thus, derived and the optimized values can be referenced from Table (4.3) and (4.4).

Using the equation (4.21), the value of Self Inductance of all 3 segments of the Lead is obtained. L_{self1}=0.534338 nH, L_{self2}=0.265657 nH, L_{self3}=0.73525 nH.

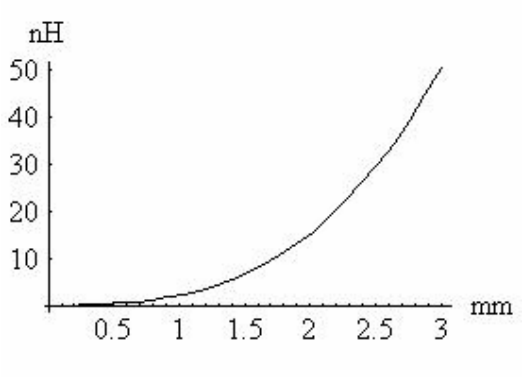

(a)t=0.2 mm where t is conductor thickness

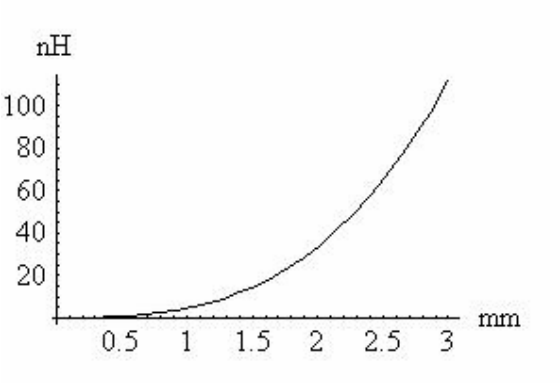

(b)t=0.09 mm where t is conductor thickness

Figure 4.7 The self-inductance extracted with the varying length of the conductor

The equation is used in Matlab as an optimizer to estimate the possible values of L and C of any package if the dimensions of the unit under test is used.

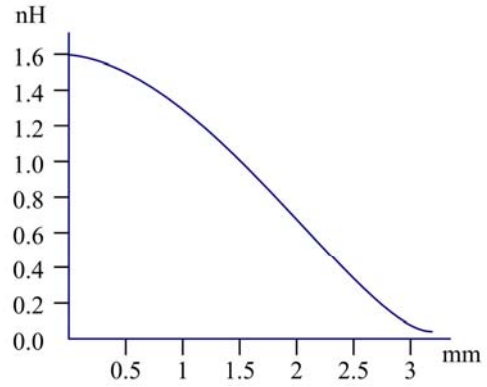

Figure 4.8 The mutual-inductance extracted with the varying width of the conductor

	Capacitance (pF)	Inductance(nH) (Self)	Inductance(nH) (Mutual)
measured data	0.6	0.9	0.4
numerical data	0.7664	0.567	0.28

Table 4.4. The comparison of capacitance and inductance of the package lead which obtained from the measured method and numerical calculation method.

From the Table, it can be seen that the value of inductance and capacitance of the Lead obtained from measured results are greater than value obtained from numerical method. Although, the capacitance is not very much different in both method, we can see that the inductance has quite different values, since we have assumed the Lead as a single transmission line.

Chapter 5

Conclusion

For Microwave and RF packaging, a good package design ensures low-cost solutions. Thus, development of characterization techniques for surface mounted package plays an important role in the electronic communications industry.

Characterizing multi-conductor leads, most especially, the coupling effect between near neighboring pins of the microwave and RF packages was performed. For the first step, the interconnects enabling the proper transitions between the package lead and wafer-probes are designed using the HP-MDS and IE3D, Zealand Software for 2D planar structure and fabricated using photolithography technique.

With the structures designed, the sets of the electrical parameters of the TSSOP package are extracted using TRL calibration method. With the collected data, the lump element model and transmission line model have been extracted. Unique Calibration method has been proposed in this thesis and based on this method, low-cost characterization of plastic packages could be modified.

Table 4.8 compares the values of capacitances and inductances of the package by measurement and numerical model. The mutual inductance and coupling capacitance are extracted based on theoretical model and physical dimension of the leads. The results vary since in numerical modeling, the dispersion effect is neglected. The package is calibrated of the bandwidth of 6 GHz (1 GHZ~ 6 GHz).

Many factors and considerations have been taken into accounts. Such factors includes the choice of the correct substrate for the correct device, and correct calibration techniques for certain type of measurements. Another factor playing significant part determining the parasitic values is the loading and proper grounding of the package. When considered as a multiport microwave network using CPA with lower dielectric loss, the electrical model should have different quantities and could obtained more accurate model.

In this thesis, TRL calibration in conjunction with the TSSOP has been chosen to study the technique of characterization of the packages. With this technique, the parasitic behavior of the packages can be predicted so as to enhance the design the MMIC circuits as well as other faster clock speed circuits.

Photolithography Procedures

Applying Photoresist

1. Make sure that only red light is on.
2. Place the substrate onto the spinner's chunk, circuit side up.
3. Using a clean treat pipette, apply about 5 droplets of photoresist onto the substrate.
4. Spin the substrate for 30 seconds at 5000 rpm to deposit an even layer of photoresist.
5. Bake the substrate for 8 minutes at 70 C, in order to cure the photoresist.
6. Let the substrate cool down.

Exposure

1. Warm up the UV light for 10 mins.
2. Place the mask on the top of the substrate clamp stand. Clamp the substrate with a clear glass plate.
3. Expose the photoresistive layer to UV light for 2 mins.

Developing

1. Place the substrate in the recommended diluted photoresist developer for 15 sec. Observe the substrate , a circuit pattern cloud of photoresist should rise from the substrate.
2. Immediately, place the substrate in a beaker of distilled water and agitate for a few seconds.
3. Gently, blow any water from the substrate with a gas get (normally we don't use gas jet, just let it dry a while) and observe the line definition and dimensions of the photoresistive lines under a non-illuminated microscope.
4. Post-bake the substrate for 20 mins at 120 ˚C .
5. After baking, leave the substrate on the workbench for about 1 mins to cool down.

Gold Etching

1. The white light was switched on.
2. Cover the ground plane with adhesive plastic tape.
3. The gold etch solution was placed on the hot plate and adjust the temp to 40 C.

For 1 mins and 30 sec was used for etching and substrate was placed in a distilled water bath. If etching is incomplete , etch for another 30 sec.

1. The test picece was washed under gently running distilled water(tap water could be used) for 5 mins.
2. The circuit was observed under microscope if there were any remains of gold at the edges, and a scalpel was to clean and if necessary, etching was continued.(normally, the desired part was covered with stickytape, and etch again).

Nichrome / Chrome Etching

1. The substrate was in the Nichrome/Chrome etch at the room temp (25 C) for 45 sec.
2. Observe the circuit pattern coming out.
3. Wash gently under running water for 5 minutes.

Cleaning

1. Acetone was to remove the photo resist on the surface of substrate .
2. The plastic tape was removed on the ground plane.

For alumina substrate with gold conductor, the process of both gold etching as well as nichrome etching procedures were used..

For Taconic substrate or Duriod substrate with copper conductor, only the copper etching procedure was used instead of gold and nichrome etching , then do the cleaning.

Copper etching.

The 400mil of distilled water with 4 spoon(table spoon)of Sodium Peroxidisulfate($Na_2O_8S_2$) with M-238.09 g/mole was mixed.

The beaker was put on the hotplate of 40 C and etch until the pattern u want is developed.

Nichrome Etching

The necessary solutions for nichrome etching are as follows:

-1000ml of Distilled water

-35 ml of Glacial Acetric Acid

-150 g of Cereic Ammonium Nitrate

$C_c(NH_4)2(NO_3)6$

Temp: 25 degree +/- 5 degree C

Gold Etching

-400 g of Potassium Iodide KI

-100 g of Iodine I_2

- 400 ml of Distilled water

- Dissolved KI and I_2 to make 400 ml of solution

Temp: 45 degree +/- 5 degree C

REFERENCES

[1] C. Chun, et al., " Development of Microwave Package Models Utilizing On-Wafer Characterization Techniques," IEEE Trans., Vol MTT-45,Oct 1997,pp.1948-1954.

[2] D. F. Williams and D. K. Walker," In-Line Multiport Calibration Algorithm," Publication of the National Institute of Standards and Technology.

[3] A.E. Ruehli, "Inductance Calculations in a Complex Integrated Circuit Environment", IBM Journal, September, 1972.

[4] D. E. Carlton, K. R. Gleason and E. W. Strid, "Microwave Wafer Probing," Microwave Journal, January 1985.

[5] Dylan Williams," De-embedding and Unterminating Microwave Fixtures with Nonlinear Least Squares", IEEE Transc., MTT, Vol., 38, No.6,June 1990.

[6] Takao Komuro, " Time-Domain Analysis of Lossy Transmission Lines with Arbitrary Terminal Networks," IEEE Transc., Circuits and Systems, Vol. 38, No.10, October 1991.

[7] J. S. McLean and Tatsuo Itoh, " Analysis of New Configuration of Coplanar Striplines," IEEE Trans. MTT Vol., 40, No.4, April 1992.

[8] R. B. Mark and D. F. Williams, " A general waveguide circuit theory," J. Res. Natl. Inst. Stand. Technol., Vol.97, pp.533-561,Sept.-Oct. 1992.

[9] D. F. Williams and R. B. Marks, " Calibrating On-Wafer Probes to the Probes Tips," 40th ARFTG Conference Digest, pp.136-143,Dec.1992.

[10] Ching-Chao Haung," Exploting Symmetry In the Extration of Electrical Packaging Parameters." IEEE Transc., 1993.

[11] K. Beilenhoff, H. Klingbeil, W. Heinrich and H. L. Hartnagel, “ Open and Short Circuits in Coplanar MMIC’s “, IEEE Trans, MTT, Vol.,41,No.9, September 1993.

[12] Cascade Microtech, Inc., Technical Brief,” A Guide to Better Vector Network Analyzer Calibrations for Probe-Tip Measurements”, 1994.

[13] P. Pogatzki, R. Kullke, D. Kother, R. Tempel and I. Wolff,” A Comprehensive Evaluation of Quasi-Static 3D-FD Calculations for more than 14 CPW Structures-Lines, Discontinuties and Lumped Elements, IEEE Transc., MTT-S Digest, 1994.

[14] Chi-Taou Tsai, “ Package Inductance Characterization at High Frequency,” IEEE Transc., Packaging and Manufacturing Technology: Advanced Packaging, Vol., 17, No.2, May 1994.

[15] Jamie Pla,Wyane Struble, and Francois Colomb,” On-Wafer Calibration Techniques for Measurement of Microwave Circuits and Devices on Thin Substrates”,1995 IEEEE MTT-S Digest.

[16] Albert Ruehli, Clayton Paul and Jan Garrett,” Inductance Calculations using Partial Inductances and Macromodels,” IEEE Transc, 1995.

[17] Hisanori Uda, Tetsuro Sawai, and Yasoo Harada,” A Novel Method to Determine Equivalent Circuits for MMIC Plastic Packages Using Electromagnetic Field Simulation,” MOTL, Vol., 10.No.3, October 1995.

[18] F. Leferink,” Inductance Calculations: Methods and Equations,” 1995 IEEE International Symposium on Electromagnetic Compatibiltiy.

[19] C. T. Tasi, W. Y. Yip, “ An Experimental Technique for Full Package Inductance Matrix Characterization,” IEEE Transc, Comp., Packaging and Manu. Tech., Vol.19, No.2,1996, pp.338-343.

[20] A. Pham, et al., " Development of a Surface Mountable Plastic Package Characterization Techniques," IEEE Transc, MTT-S Digest,1996,pp.147-149.

[20] R. W. Jackson, " A Circuit Topology for Microwave Modeling of Plastic Surface Mount Packages," IEEE Transc., MTT, Vol.,44, No.7, July 1996.

[21] D.F. Williams, "Calibration in multiconductor transmission lines," in 48th ARFTG Conf. Dig., Orlando, FL, Dec. 4-6, 1996.

[22] D. F. Williams, Jean-Maxence Belquin and Gilles Dambrine and Randy Fenton," On-Wafer Measurement at Millimeter Wave Frequencies," 1996 IEEE Transc., MTT-S Digest.

[23] A. Pham, J. Laskar, G. Zhou and Brain Hutchinson," Development of a Surface Mountable Plastic Package Characterization Technique," IEEE Transc., 1996.

[24] B. Krauter and L. T. Pileggi,' Generating Sparse Partial Inductance Matrices with Guaranteed Stability," IEEE Transc., 1995.

[25] R. B. Marks and D. F. Williams," Interconnection Transmission Line Parameter Characterization," Publication of the National Institute of Standards and Technology.

[26] Carl Chun, Anh-Vu Pham, Joy Laskar and Brain Hutchison, " Development of Microwave Package Models Using On-Wafer Characterization Techniques", MTT Vol.,45,No.10, October 1997.

[27] A. Pham, et al., " Surface Mount Microwave Package Characterization Technique," IEEE MTT-S,pp.995-998, 1997.

[28] D. F. Williams, "Multi-conductor transmission line Characterization," in IEEE Trans., Comp., Pack., and Manuf., Technol.-Part B,Vol. 20,N0. 2,pp.129-132, May 1997.

[29] D.F. Williams, "Characterization of embedded multi-conductor transmission lines," in IEEE /MTT-S Int. Microwave Symp. Dig., June 10-12, 1997.

[30] Christopher L. Holloway and Edward F. Kuester," Net and Partial Inductance of a Microstrip Ground Plane," IEEE Transc., Electromagnetic Compatibility , Vol.40, No.1, February 1998.

[31] C. Seguinot, P. Kennis, Jean-Frabucis Keguerm, F. Huret, E. Paleczny and L. Hayden," Multimode TRL-A New Concept in Microwave Measurements:Theory and Experimental Verification," IEEE Transc., MTT, Vol.46, No.5, May 1998.

[32] M. Beattie, L. Alatan and L. Pileggi," Equipotential Shells for Efficient Parital Inductance Extraction," IEEE Transc., 1998.

[33] R. M. Simon and G. E. Ponchak," Modeling of Some Coplanar Waveguide Discontinuities," IEEE Transc., MTT. Vol.36, No.12, December 1998.

[34] D.F. Williams, J.E. Rogers, and C.L. Holloway, " Multi-conductor Transmission-Line Characterization: Represen-tations, Approximations, and Accuracy," IEEE Trans., Vol, MTT-47, No. 4, April 1999.

[35] A. J. Dammers and N. P. van der Meijs," Virtual Screening: A Step Towards a Sparse Partial Inductance Matrix," IEEE Transc, 1999.

[36] M. W. Beattie and L. T. Pileggi," IC Analyses Including Extracted Inductance Models," 1999.

[37] C. L. Hammond and Kathleen L. Virga, " Network Analyzer Calibration Methods for High-Density Packaging Characterization and Validation of Simulation Models", 2000 Electronic Components and Technology Conference.

[38] D.J. Bnnister and D.I. Smith, " Traceability For On-Wafer CPW S-Parameter Measurements," National Physical Laboratory, Worcs WR 14 3ps.

[39] Vincent Leong Yoke Choy," Thru-Reflect-Line : Calibration Technique For Vector Network Analyzer," Defence Science Organization, Singapore.

[40] " Network Analysis , Applying the HP8510 TRL Calibration for non-coxial measurements," Product Note 8510-8A, Hewlett Packard.

[41] David M. Pozar," Microwave Engineering," 2nd edition.

[42] Carl T.A Johnk, " Engineering Eelectromagnetic Fields and Waves", 2nd edition.

[43] Fred Monaco," Introduction to Microwave Technology", 1989.

[44] R. K. Hoffman," Handbook of Microwave Integrated Circuits,"1987.

[45] Brian C. Wadell, " Transmission Line Design Handbook,"1991.

[46] Rajesh Mongia, Inder Bahl and Prakash Bhartia," RF and Microwave Coupled-Line Circuits,"1999.

[47] Max W. Mdeley, " Microwaave and RF Circuits: Analysis, Synthesis and Design,"1993.

[48] K.C. Gupter, " Microstip Lines and Slot Lines", 2nd edition.

[49] C.A Balanis," Advanced Engineering Electromagnetics", 2nd edition.

[50] C.A Balanis," Antenna Theory,Analysis and Design ", 2nd edition.

[51] J. A. Brandao Faria, " Multiconductor Transmission-Line Structure, Modal Analysis and Techniques," 1993.

[52] Niels Fache, Frank Olyslager,Daniel De Zutter, " Electromagnetic and Circuit Modelling of Multiconductor Transmission Lines" ,1993.

[53] Clayton R. Paul, " Analysis of Multiconductor Transmission Lines," 1994.

[54] Ruel V. Churchill and James Ward Brown," Complex Variables and Applications," 4th edition.

[55] Harlan Howe, JR, "Stripline Circuit Design",1982.

[56] David H. Schrader, " Microstrip Circuit Analysis",1995.

[57] Gene H. Golub, Charles F. Van Loan," Matrix Computions," 2nd edition.

[58] Frank Olyslager, “ Electromagnetic Waveguides and Transmission Lines”, 1999.

[59] Nihad Ibranhim Dib**, “**Characterization of asymmetric coplanar waveguide discontinuities**”,** Microwave Theory and Techniques, IEEE Transactions, Issue: 9, Sept. 1993**.**